Journal of Ethnopharmacology 349 (2025) 119915

Contents lists available at ScienceDirect

Journal of Ethnopharmacology

journal homepage: www.elsevier.com/locate/jethpharm

Asarum heterotropoides F. schmidt attenuates osteoarthritis via multi-target anti-inflammatory actions: A network pharmacology and experimental validation

Hee-Geun Jo [a,b,1], Chae Yun Baek [a,1], Sidra Ilyas [a], Yeseul Hwang [a], Eunhye Baek [c], Ho Sueb Song [d,*], Donghun Lee [a,**]

[a] Department of Herbal Pharmacology, College of Korean Medicine, Gachon University, 1342 Seongnamdae-ro, Sujeong-gu, Seongnam-si, 13120, Republic of Korea
[b] Naturalis Inc., 6, Daewangpangyo-ro, Bundang-gu, Seongnam-si, 13549, Republic of Korea
[c] RexSoft Inc., 1 Gwanak-ro, Gwanak-gu, Seoul, 08826, Republic of Korea
[d] Department of Acupuncture & Moxibustion Medicine, College of Korean Medicine, Gachon University, 1342 Seongnamdae-ro, Sujeong-gu, Seongnam-si, 13120, Republic of Korea

ARTICLE INFO

Handling Editor: Dr. Y Min

Keywords:
Osteoarthritis
GEO datasets
Molecular docking
Network pharmacology
Asarum heterotropoides F.Schmidt

ABSTRACT

Ethnopharmacological relevance: *Asarum heterotropoides* F. Schmidt (ARR) has a well-documented history of traditional use in East Asia for musculoskeletal pain disorders, including osteoarthritis (OA), attributed to its significant anti-inflammatory properties. While preliminary studies suggest potential anti-inflammatory effects, conclusive evidence regarding the ability of ARRs to modulate the multiple inflammatory pathologies involved in OA pathogenesis is currently lacking.

Aim of the study: This study aimed to experimentally evaluate the effects of ARR extract on pain, cartilage integrity, and inflammatory responses using in vitro and in vivo models relevant to OA, guided by initial computational predictions.

Materials and methods: Active ingredients of ARRs were retrieved from four databases and screened using SwissADME for ADME predictions. Disease targets were combined with OA-related genes from GEO microarray database. The intersecting genes underwent protein-protein interaction construction, GO, and KEGG enrichment analysis. A compound-target-pathway network was constructed using Cytoscape and was validated via molecular docking. Pain-relieving, functional, and chondroprotective effects were assessed in vivo using acetic acid-induced peripheral pain mice and monosodium iodoacetate (MIA)-induced osteoarthritis rat models. Furthermore, anti-inflammatory properties were explored by evaluating serum cartilage tissue and lipopolysaccharide-stimulated RAW 264.7 cells.

Results: Network pharmacology analysis elucidated five principal active constituents of ARR (cryptopine, 5-[2-(2-hydroxyphenyl)ethyl]-2,3-dimethoxy-phenol, 5-[2-(3-hydroxyphenyl)ethyl]-2-methoxybenzene-1,3-diol, naringenin, resorstatin) alongside 22 putative herbal targets. Molecular docking analyses revealed strong binding affinities (−8 to −9.4 kcal/mol) of these constituents towards principal target proteins. Functional GO and KEGG enrichment analyses indicated that ARR exerts its effects potentially involving pathways associated with cancer, fluid shear stress, and atherosclerosis. *In vivo* assessments demonstrated significant mitigation of pain, functional deficits, and cartilage degradation by ARR within an MIA-induced osteoarthritis model. Molecular dynamics simulations validated stable interactions between the primary compounds and their designated target proteins. The therapeutic efficacy of ARR was characterized by dose-dependent suppression of diverse inflammatory mediators (IL-1β, IL-6, TNF-α), matrix metalloproteinases (MMP-1, -3, -8, -13), and signaling pathways including CCND1, CDK2, IKBKB, HIF1A, BDKRB1, SIRT1, MAPK8, and NLRP3 within both RAW264.7 cells and articular cartilage tissue.

Conclusions: This investigation demonstrates that ARR exerts pain alleviation, functional enhancement, and chondroprotective effects in osteoarthritis via multi-target anti-inflammatory actions. Integrating network

* Corresponding author.
** Corresponding author.
E-mail addresses: hssong70@gachon.ac.kr (H.S. Song), dlee@gachon.ac.kr (D. Lee).
[1] These authors contributed equally to this work.

https://doi.org/10.1016/j.jep.2025.119915
Received 29 January 2025; Received in revised form 12 April 2025; Accepted 29 April 2025
Available online 7 May 2025

pharmacology, molecular docking, animal models, and cellular experiments, this study comprehensively elucidated the multifaceted anti-inflammatory mechanisms attributed to ARR. These findings collectively provide a crucial foundation for understanding the potential therapeutic efficacy and operative mechanisms of ARR for osteoarthritis management.

Abbreviations

absorption, distribution, metabolism, and excretion	ADME
Asarum heterotropoides F. Schmidt	ARR
Apoptosis associated speck like protein containing a CARD	ASC
betweenness centrality	BC
biological process	BP
bradykinin receptors beta	BDKRB
cellular component	CC
closeness centrality	CC
Collective Molecular Activities of Useful Plants	CMAUP
cyclin D	CCND
cyclooxygenase	COX
Control	CT
degree centrality	DC
differentially expressed genes	DEGs
disease-modifying osteoarthritis drugs	DMOADs
drug-likeness	DL
Distilled water	DW
East Asian herbal medicine	EAHM
Encyclopedia of Traditional Chinese Medicine v2.0	ETCM v2.0
erb B2 Receptor Tyrosine Kinase	ERBB
estrogen receptor	ESR
Gene Expression Omnibus datasets	GEO
gene ontology	GO
glyceraldehyde 3-phosphate dehydrogenase	GAPDH
high-performance liquid chromatography	HPLC
Hypoxia Inducible Factor 1 Subunit Alpha	HIF1A
Inhibitor of Nuclear Factor KappaB Kinase Subunit Beta	IKBKB
Institute for Cancer Research	ICR
indomethacin 3 mg/kg	IDM 3
interleukin	IL
Kyoto Encyclopedia of Genes and Genomes	KEGG
Linking of Traditional Chinese Medicine with Modern Medicine at Molecular and Phenotypic Levels	LTM-TCM
lipopolysaccharide	LPS
matrix metalloproteinases	MMP
maximal clique centrality	MCC
mitogen-activated protein kinase	MAPK
molecular function	MF
monoiodo-acetate	MIA
NOD/LRR and pyrin domain containing protein 3	NLRP3
nitric oxide	NO
nitric oxide synthase	NOS
non-steroidal anti-inflammatory drugs	NSAIDs
oral bioavailability	OB
osteoarthritis	OA
prostaglandin E receptor 2	Ptger2
sirtuin	SIRT
Sprague-Dawley	SD
Traditional Chinese Medicine Systems Pharmacology Database and Analysis Platform	TCMSP
tumor necrosis factor	TNF
weight-bearing ratio	WBR

1. Introduction

Osteoarthritis (OA), the most common arthropathy, is clinically defined by enduring pain, sustained inflammation, progressive and irreversible articular cartilage degradation, and subsequent disease advancement, ultimately resulting in functional disability and a spectrum of associated comorbidities(Mahmoudian et al., 2021). The societal burden of OA, an age-related disease, is rapidly increasing as obesity and aging become global health concerns. The World Health Organization predicts that by 2030, OA will significantly contribute to increased mortality and healthcare costs owing to the marked rise in the population aged 60 years and older (Scott et al., 2021; Tchkonia et al., 2021). Epidemiological studies have indicated that the global prevalence of OA has surged by 113.25 %, from 247.5 million in 1990 to 527.1 million in 2019. Additionally, productivity losses due to OA were estimated to be $60.7 billion in 2019, underscoring the growing public health challenge posed by the disease worldwide (Long et al., 2022; Weng et al., 2024). Until recently, the pathophysiology of OA was understood to involve solely degenerative changes in the articular cartilage due to aging and biomechanical stress. Recent human and animal studies have accumulated evidence that low-grade chronic inflammation plays a central role in the progressive pathology of OA, leading to pain, joint failure, and irreversible destruction of the entire joint (Robinson et al., 2016; Sanchez-Lopez et al., 2022). Therefore, recent therapeutic approaches to OA have focused on developing interventions that can potentially delay or modify the ongoing inflammatory pathology and consequent disease progression.

Despite significant advances in our understanding of the pathophysiology of OA, which is now centered on inflammation, there are currently no drugs that can halt disease progression or completely prevent long-term disability (De Roover et al., 2023). In light of these considerations, leading clinical practice guidelines advocate for non-pharmacological interventions, including weight reduction, therapeutic exercise, and physical rehabilitation, as the primary management strategy for OA (Yao et al., 2023). In terms of pharmacotherapy, non-steroidal anti-inflammatory drugs (NSAIDs), glucocorticoids, and opioids are used to alleviate disease symptoms, primarily pain. However, these drugs do not inhibit OA progression, and the most widely used NSAIDs are associated with a wide range of long-term toxic side effects (Katz et al., 2021). Consequently, there is a need for additional alternatives to improve the effectiveness and safety of current OA therapies. Disease-modifying osteoarthritis drugs (DMOADs), representing a newly emerging class of therapeutics, have been proposed as a promising strategy. These pharmacological agents are designed to impede the advancing pathophysiology of OA through the modulation of diverse molecular targets, encompassing pro-inflammatory cytokines, matrix metalloproteinases, and nociceptive pathways associated with OA-related pain (Latourte et al., 2020). Recently, the recognition that senescent cells, which accumulate with aging, are significant triggers of chronic low-grade inflammation and OA progression, has led to the proposal of a class of drugs called senolytics, which selectively remove these cells from the joint tissue (Chaib et al., 2022). Unfortunately, to date, no DMOADs have been approved by regulatory agencies or reached the market.

This connection is associated with the continually recognized systemic and multifaceted nature of OA pathology. The understanding of OA has evolved beyond mechanical 'wear and tear' to recognize it as a complex immune-mediated disease involving innate and adaptive systems(Moulin et al., 2025). Local joint inflammation, driven by synovial immune cells producing pro-inflammatory cytokines and matrix-degrading enzymes, contributes to cartilage destruction and pain (Wen et al., 2024). This pathology is exacerbated by systemic low-grade inflammation associated with metabolic inflammation and inflammaging, involving adipokines and senescent cells(Jamal et al., 2025). Autoimmune mechanisms are implicated, with autoantibodies against synovial and cartilage components observed in advanced OA(Paiola et al., 2025). Emerging evidence also highlights a gut-joint axis, where gut dysbiosis potentially promotes OA progression via increased circulating lipopolysaccharides and altered tryptophan metabolism(Yang

et al., 2024). Consequently, there is a critical need for investigations into novel therapeutic candidates capable of reflecting the full scope of OA pathology considered as a systemic inflammatory condition.

One critical requirement for a successful DMOAD candidate is the capacity to modulate multiple targets of inflammatory pathology in OA, including various cytokines such as interleukin (IL)-1, IL-6, IL-8, tumor necrosis factor (TNF)-α, and proteases such as matrix metalloproteinases (MMPs) (Lu et al., 2022; Van Spil et al., 2019). Natural products with demonstrated pharmacological activities can meet this demand by leveraging their unique multicomponent-based anti-inflammatory mechanisms and synergistic effects among multiple components (Panossian et al., 2015, 2021, 2024; Su et al., 2023). Particularly, East Asian herbal medicine (EAHM) has garnered attention as a source of drug candidates for inflammatory joint diseases, attributed to its long-standing safety profile, theory of synergistic drug combinations, cost-effectiveness, and active scientific research (Fang et al., 2024; H.-G. H.G. Jo et al., 2023; H. G. H.-G. Jo et al., 2023; Jo et al., 2025, 2024a, 2024b, 2022, 2020; Li et al., 2023). Among the numerous EAHMs, *Asarum heterotropoides* F. Schmidt (Latin name: Asiasari Radix et Rhizoma, ARR) stands out as a promising candidate material for the treatment of joint diseases due to its anti-inflammatory properties. It has a history of use in alleviating joint pain, stiffness, and improving function (Liu and Wang, 2022). It has been documented that this medicinal plant possesses analgesic, neuroprotective, anti-ischemic, immunomodulatory, anti-allergic, antitumor, and antimicrobial effects, along with a broad spectrum of anti-inflammatory activities attributed to its multifaceted pharmacological components (Jing et al., 2017; Liu and Wang, 2022). ARR contains over 277 compounds, primarily bioactive volatile oils (e.g., methyleugenol, safrole, asarones) and lignans (e.g., asarinin, sesamin), along with phenanthrenes, flavonoids, and amides. It demonstrates analgesic, anti-inflammatory, and neuroprotective effects by inhibiting Na^+ channels, activating GABA receptors, and suppressing pro-inflammatory cytokines and pathways like NF-κB/MAPK. Its lignans and volatile oils also offer cardiovascular protection through antithrombotic activity and modulation of endothelial protein C receptor shedding. While high doses of volatile oils and trace aristolochic acid analogs pose toxicological risks, recommended dosages and traditional decoction methods mitigate these concerns. Despite the potential of ARR as a DMOAD, comprehensive studies analyzing its viability as a candidate for treating osteoarthritis are scarce.

Considering these factors, we hypothesized that ARR might represent a promising DMOAD candidate, potentially hindering the progression of OA due to its multi-component, multi-target, and anti-inflammatory pharmacological profile. To investigate this hypothesis, we employed network pharmacology and molecular docking analyses to predict the mechanisms by which ARR's primary constituents and their targets could modulate osteoarthritis. Subsequently, we validated the anti-inflammatory effects of ARR on various targets based on the predicted results in *in vitro* models and assessed its impact on analgesia, chondroprotection, and functional improvement in OA in *in vivo* models. This study represents the first comprehensive investigation into the anti-osteoarthritis potential of ARR by integrating network pharmacology predictions with experimental validations. This dual approach not only bridges computational insights and experimental evidence but also sets a new idea for exploring multi-target therapeutics in OA research.

2. Materials and Methods

2.1. Network pharmacology prediction for ARR in OA

2.1.1. Screening of potential ARR active components and target identification for OA

To identify the potential bioactive components of ARR, we employed a strategy involving four established databases. Initially, the Traditional Chinese Medicine Systems Pharmacology Database and Analysis Platform (TCMSP), a widely recognized resource in network pharmacology, was utilized. Subsequently, to incorporate recent advancements in pharmacological data, we incorporated Linking of Traditional Chinese Medicine with Modern Medicine at Molecular and Phenotypic Levels (LTM-TCM), Collective Molecular Activities of Useful Plants (CMAUP), and Encyclopedia of Traditional Chinese Medicine v2.0 (ETCM v2.0) as contemporary platforms(Hou et al., 2023; Li et al., 2022; Lu et al., 2021; Ru et al., 2014; Zeng et al., 2019; Zhang et al., 2023). Furthermore, the PubChem database was used to standardize the retrieved compounds from each database and to remove any redundancies.

For compounds sourced from the TCMSP DB, selection was performed based on established thresholds of oral bioavailability (≥30 %) and drug-likeness index (≥0.18). Compounds obtained from alternative databases underwent screening for absorption, distribution, metabolism, and excretion (ADME) properties utilizing the SwissADME platform (http://www.swissadme.ch) (Daina et al., 2017). The selection principle prioritized compounds that received a "yes" evaluation in a minimum of three out of the five ADME rule sets (Lipinski, Ghose, Veber, Egan, and Muegge). However, compounds were excluded if any single evaluation parameter within the Lipinski rule was violated. To predict potential targets, the SwissTargetPrediction platform (http://www.swisstargetprediction.ch) was employed, configured for "Homo sapiens," and target genes were considered for further analysis if their prediction probability was ≥0.1(Daina et al., 2019).

2.1.2. Building the database of potential therapeutic disease targets

To obtain mRNA expression profiles for osteoarthritis (OA) and normal control samples, we queried the Gene Expression Omnibus (GEO) database. The search strategy employed utilized the terms "osteoarthritis" [MeSH terms] OR osteoarthritis [all fields]) AND "Homo sapiens" [porgn]. Subsequently, the GSE46750 expression dataset, derived from the GPL10558 microarray platform (Illumina HumanHT-12 V4.0 expression beadchip), was downloaded from GEO. Differential gene expression analysis between OA patients and healthy individuals was conducted using the 'limma' package in R software (version 4.1.2), with significance defined as $p < 0.05$ and an absolute log2 fold change ($|\log2\ FC| > 1$. Visualization of differentially expressed genes (DEGs) was achieved through heatmaps and volcano plots, generated using the 'Pheatmap' and 'ggplot2' R packages. Furthermore, to identify OA-related target genes, we performed a search across four databases: DrugBank, GeneCards, OMIM, and TTD, employing the search terms "osteoarthritis" and "oa"(Amberger et al., 2019; Piñero et al., 2015, 2017, 2020; Wishart et al., 2018; Zhou et al., 2023). Within GeneCards, only targets with a relevance score of ≥10 were considered(Stelzer et al., 2016). To standardize potential target gene information, the "Homo sapiens" filter within the UniProt database was applied (The UniProt Consortium, 2021). Ultimately, a dataset of potential OA target genes was compiled following the removal of redundant entries. Venn diagrams illustrating the overlap of targets between potential ligands and target disease were generated using the Bioinformatics & Evolutionary Genomics web-based tool.

2.1.3. Construction of protein-protein interaction (PPI) networks

We generated a protein-protein interaction (PPI) network for the identified shared targets utilizing the STRING database (version 11.5) and applying a confidence score threshold of 0.4 or higher. Prior to topological analysis, non-relevant protein nodes were eliminated, and the resulting data were imported into Cytoscape (version 3.9.1) along with the Cytohubba plug in (Chin et al., 2014; Shannon et al., 2003). Hub genes were then determined by considering the union of targets that ranked within the top 25 % for each of the following four centrality measures: degree centrality (DC), betweenness centrality (BC), closeness centrality (CC), and maximal clique centrality (MCC).

2.1.4. Gene ontology (GO) and Kyoto encyclopedia of genes and genomes (KEGG) analysis

Enrichment analysis of genes was performed utilizing Metascape, a

web-based resource for gene function annotation (Zhou et al., 2019). Specifically, analyses were restricted to "Homo sapiens," with a *p*-value cutoff of 0.01 and a minimum overlap of three for enrichment. Within Metascape, we analyzed the gene symbols of the shared targets to determine their functional enrichment across biological processes (BP), cellular components (CC), molecular functions (MF), and KEGG pathways. To further investigate the molecular underpinnings of core pathways identified through enrichment, the KEGG mapper tool was employed (Kanehisa et al., 2022).

2.1.5. Establishment of compound-target-pathway (C-T-P) network

Employing Cytoscape, we constructed a compound-target-pathway (C-T-P) network model to elucidate the therapeutic mechanisms of ARR in OA, visually representing the interconnections among its constituents, genomic targets, and relevant biological pathways. Furthermore, we selected the key compounds and targets expected to play the most important roles in the efficacy of ARR's against OA based on the degree centrality metric calculated at the time of network construction, which was more than three times the median.

2.1.6. Molecular docking verification

The 3D structures of the target protein molecules were obtained in PDB format using the RCSB PDB database. Proteins were prepared for docking using the UCSF chimera software (version 1.17.3). Medicinal drug compounds as ligands were downloaded from the PubChem. Ligand smile strings and prepared proteins were uploaded to the online drug discovery platform, mcule (https://mcule.com/). The binding energy predicted using mcule was recorded, and the docked structures were downloaded. Discovery Studio 2021software was used to assess the docking outcomes of the target proteins and medicinal drug compounds, and for 2D visualization. For each compound, results with a binding free energy (ΔG) of −5 kcal/mol or lower were considered significant.

2.2. Preparation of ARR extracts

The ARR root used in these experiments was bought from Yaksudang Corp. (Seoul, Korea). The voucher specimen was stored in the Herbal Medicine Department, Korean Medicine College and Gachon University. A prof. Donghun Lee were authenticated (No. D200915012). The root sample (10 g) was finely ground and extracted using a reflux method (85 °C, 3 h and 30 % ethanol). After filtration, the extract was concentrated and freeze dried in the deep freezer. The extraction yield was 13.02 %.

2.3. HPLC

To analyze the components of ARR, HPLC was conducted using an Agilent 1100 series HPLC system (USA). The specific analytical conditions are detailed in Supplementary Material S1.

2.4. Animals

The male SD rats (200 ± 10 g) was utilized as an OA induced model, while male ICR mice (35 ± 5 g) were utilized the hot plate and writhing responses test. The animals were provided by DBL, Co., Ltd. with 45 rats assigned to OA model and the 40 mice allotted with hot plate and writhing tests for each experiment. Prior to the experiment, the animals were kept in a controlled environment for 7 days to ensure proper acclimatization (temp:20–24 °C, humidity: 50–60 %, dark/light cycle: 12-h). Water and food were supplied *ad libitum*. All experimental process strictly adhered to the Institutional Animal Care & Use Committees (IACUC) of Gachon University (GU1-2022-IA0071-01) and complied with the ARRIVE 2.0 guidelines (Supplementary Material S2) [47].

2.5. Diet preparation and monosodium iodoacetate (MIA) injection

The five groups of SD rats (n = 9) were vehicle, CT, IDM 3, ARR 100, and ARR 300. The rats were given intraarticular injections of MIA (Sigma, USA) for establish OA. The experimental groups were fed the following diets: basic food (AIN93G) for the vehicle and CT groups. The IDM group received AIN93G diet with indomethacin (0.003 %). The ARR 100 and ARR 300 groups received AIN93G diet with ARR (0.11 and 0.33 %). For 24 consecutive days following MIA induced OA, the animals were provided with a diet of 18–22 g per 180–220 g of body weight on a basis daily (Supplementary Material S3).

2.6. Measuring weight bearing ratio (WBR) of hind legs

To determine the WBR of the hind legs in the OA induced models, the WBR was measured every 3 days during 24 days recording with incapacitance tester (IITC Life Science Inc., USA). After each group were received drug administration daily, each hind limb was weighted and placed on the incapacitance tester during 10 s to calculate the WBR. The percentage improvement in the right legs WBR was analyzed the following formula:

$$\text{WBR}\ (\%) = \frac{\text{right hind limb's weight}}{\text{both hind limb's weight}} * 100$$

2.7. Cartilage degradation assessment

After 24 days, the OA induced models were sacrificed, and their knee cartilage of right side were photographed and evaluated through macroscopic scoring. Photos were captured by the digital camera (SonyCorp., Japan), and the extent of cartilage and bone degradation was scored following the macroscopic score (Supplementary Material S4).

2.8. Serum concentration analysis

Blood was collected from the abdominal vein and allowed to clot for 30 min. The sample was centrifuged at 4000 rpm for 10 min, and the serum was subsequently isolated and preserved in a deep freezer. For cytokine analysis, multiplex assays were conducted using an IL-1β Multi-Analyte Premixed Kit (RnD Systems Inc., USA). Cytokine levels were assessed with a magpix analyzer (Luminex Corp., USA), following protocol of manufacturer.

2.9. Writhing test

The animals used in the writhing test were assigned to 4 groups of eight animals each group randomly. The groups were as follows: control (CT), ibuprofen (IBU 200), ARR 200, and ARR 600. Each group was orally administered DW, ibuprofen (Sigma, USA) 200 mg/kg, ARR 200 and 600 mg/kg for the CT, IBU 200, ARR 200 and 600 groups respectively. The positive control was used with ibuprofen. 30 min following oral administration, an acetic acid (0.7 %) was injected intraperitoneally, and the number of writhing responses was recorded over a 10-min period. The number of witnesses was quantified by recording the twisting response by extending the hind paw backward or contracting the abdominal wall. All samples were made with DW. Animals were euthanized with CO_2 at the end of the experiment.

2.10. Hot-plate test

The animals used in the hot plate test experiment were randomly allotted to ICR mice to form four groups of eight animals per group. The following groups were used: control (CT), positive control (morphine), ARR 200 and ARR 600. The CT, ARR200, and ARR 600 groups were administered DW orally. The positive control was used with morphine

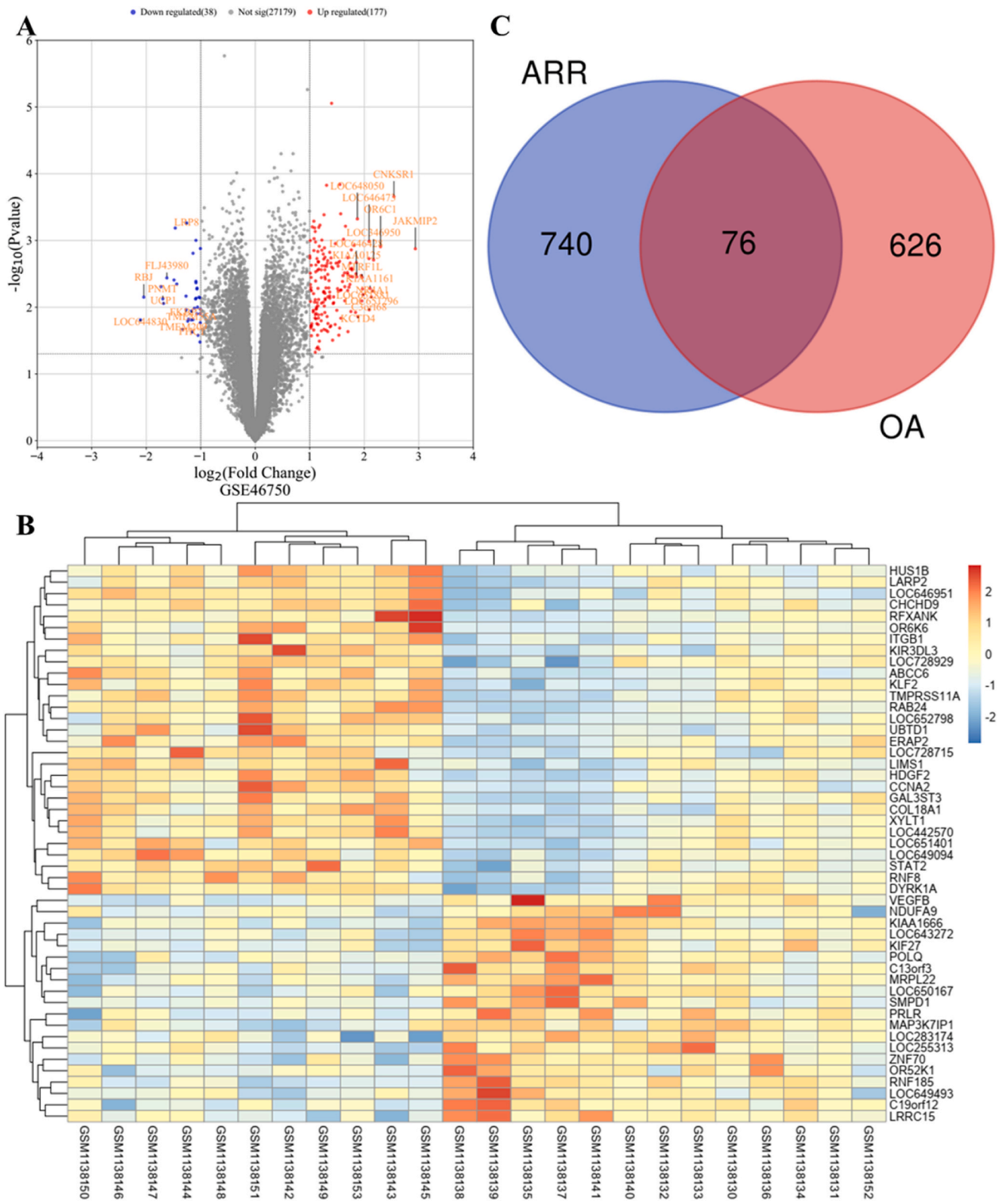

Fig. 1. Screening of ARR-targeted disease intersection targets. (A) Volcano plot of differential gene analysis in the GSE 56750 disease sample chip. Genes that are upregulated are shown in red, downregulated genes are shown in blue, and no significant changes are shown in black. (B) Heatmaps were used to display the expression patterns of these 225 DEGs. (C) Venn diagram illustrating the overlap between potential ARR targets and known OA disease targets. (For interpretation of the references to color in this figure legend, the reader is referred to the Web version of this article.)

(Myungmoon Pharm Co., Ltd., Seoul, Korea) at 10 mg/kg intraperitoneally. Thirty minutes after sample administration, licking, jumping, and shaking responses were measured on a hot plate at 55 °C for 30 s, with four measurements taken at 30 min intervals. The duration of the first response was also recorded. All samples were made in the DW. Animals were euthanized with CO_2 at the end of the experiment.

2.11. Cell culture

RAW264.7 cells were provided by Korean Cell Line Bank (KCLB; Seoul, Korea). The RAW264.7 cells were incubated on the CO_2 incubator (Thermo Fisher Scientific Inc., USA) in DMEM in 10 % FBS with 5 % penstrep (Gibco BRL, USA).

2.12. Cell toxicity and NO production test

RAW264.7 cells were maintained at CO_2 incubator for 24 h. The cells were then exposed to 10–300 μg/mL of ARR along with LPS 500 ng/mL and further incubated for another 24 h. Cell toxicity was assessed with EzCytox (DoGenBio, Korea) in accordance with the protocol. To measure NO levels, the cell supernatant was combined with Griess reagent in equal proportions (1:1 ratio), and the absorbance was recorded at 540 nm. Each experiment was performed three times for accuracy.

2.13. DCFH-DA assay

1×10^4 cells/well were cultured in the CO_2 incubator for 24 h. The cells were then treated with 10–300 μg/mL of ARR and incubated for 2 h. After the 2 h incubation, 10 μM DCFH-DA was added to the medium and incubated for 30 min. The plate was washed using PBS. Subsequently, the cells were treated to 500 μM H_2O_2 for 30 min. Finally, the plate was placed in a fluorescence reader, and was measured (excitation: 485 nm/emission: 535 nm).

2.14. Quantitative real-time PCR analysis

OA induced cartilage of rats and the LPS-induced RAW264.7 cells were extracted total RNA by the RNA-Extraction solution (Bioneer, Korea). The RNA was changed to the cDNA by Cycle-Script™ (Bioneer, Korea), using the protocol of manufacturer. Quantification of mRNA expression level was conducted by qPCR Master-Mix (Bioneer, Korea). The primer information was listed in Supplementary Materials S5 and S6.

2.15. Western blotting analysis for protein expression

Cartilage tissues of OA induced knee and LPS-treated RAW264.7 cells were isolated protein with RIPA buffer (CST Inc., USA) supplemented with Protease Inhibitor (Sigma, USA). Homogenization was performed using a D1000-E homogenizer (Benchmark, USA). Protein qualification was recorded with BCA kit (Thermo Fisher Scientific Ltd, USA), and protein were separated via SDS-PAGE. The proteins were transported onto the membrane by the Wet Transfer (BioRad Inc., USA) at 100 V and 1 h. Following transfer, the membrane was blocked with blocking solution (BioRad, USA) and incubated at 25 °C for 15 min. Primary antibodies were incubated at 4 °C for overnight. Primary antibodies were listed the MMPs, IL-1β, IL-6, TNF-α, COX-2, CCND1, CDK2, IKBKB, HIF1A, BDKRB1, SIRT1, MAPK8, NLRP3, ASC, caspase-1, and GAPDH. The antibodies were bought by Abcam and CST Inc. (Cambridge, UK and Danvers, USA). The membrane was attached with secondary antibodies at for 1 h at 25 °C, and then applied with a ECL solution (BioRad, USA). The protein signals were detected using an Azure 280 imaging system (AzureBiosystems, USA).

2.16. Molecular dynamics

To elucidate the dynamic behavior of protein-ligand complexes, molecular dynamics (MD) simulations were conducted. Initially docked complexes were parameterized using the CHARMM36 all-atoms force field, providing a detailed representations of atomic interactions. The complexes were then solvated in a cubic water box, employing the TIP3p water model, with a 12 Å buffer distance to minimize the boundary effects (Huang and MacKerell, 2013). Ligand topologies were generated using the CGenFF server (https://cgenff.com/) and subsequently adapted for compatibility with the Gromacs 2024.1 simulation package. To ensure system neutrality, appropriate numbers of sodium (Na+) and chloride (Cl-) ions were added. Energy minimization was performed using the steepest descent algorithm, converging to the gradient tolerance of 0.001 kJ/mol, thereby relaxing unfavorable initial contacts. Equilibration was achieved through temperature and pressure control, employing the Nose-Hoover thermostat and Parrinello-Rahman barostat, respectively(Bussi et al., 2007). Short-range electrostatic and van der Waals interactions were computed within a 1.2 nm cut off radius, while long-range electrostatic interactions were handled using the particle mesh Ewald (PME) method(Essmann et al., 1995). Production MD simulations, spanning 200ns, were executed for each complex using Gromacs 2024.1 (https://www.gromacs.org/). Trajectory analysis was performed using built-in Gromacs tools and structural visualizations were generated to interpret the dynamic behavior of the protein-ligand complexes (Abraham et al., 2015).

2.17. Statistics

Data were analyzed using GraphPad Prism® 9.0 (GraphPad Software, USA), employing one-way ANOVA followed by Dunnett's post hoc test. Statistical significance was defined at $p < 0.05$, with results expressed as mean ± standard error of the mean.

3. Results

3.1. Network pharmacology-based prediction of ARR mechanisms in OA

3.1.1. In silico identification of putative bioactive compounds and therapeutic targets

Ingredients collected from the four databases, TCMSP, CMAUP, LTM-TCM, and ETCM 2.0 were selected based on the ADME screening criteria, resulting in a total of 204 potentially active compounds. Compound names, PubChem CIDs, InChlKeys, CASs, and ADME evaluations are listed in Supplementary Material S7. After predicting target genes using the Swiss Target Prediction database and removing duplicates, we performed standardization using the UniProt database and constructed a target database of 3392 ARRs. Supplementary Material S8 summarizes the UniProt names, symbols, ID, and prediction probabilities of predicted targets for each compound. Compounds with no predicted targets (probability greater than 0.1) were excluded from the network analysis.

3.1.2. Identification of OA related targets

By comparing the expression levels of genes in OA and normal samples, we searched for DEGs in OA samples. A total of 225 genes were identified by analyzing the GSE46750 series, of which 177 were upregulated and 38 were down-regulated in OA(Supplementary Material S9). Fig. 1A depicts a volcano plot, visually representing the dispersion of DEGs. Fig. 1B shows heat maps of the top 50 expression patterns of these DEGs. After excluding genes that could not be standardized using the UniProt database, 167 potential targets were identified from GEO data. By integrating data from DrugBank, Genecards, OMIM, TTD, DisGeNET, and GEO DEGs, we built a database containing 871 OA targets (Supplementary Material S10). Finally, intersection mapping utilizing a Venn diagram of 816 herb gene targets and 702 OA-related targets with duplicates removed identified 76 consensus genes as potential

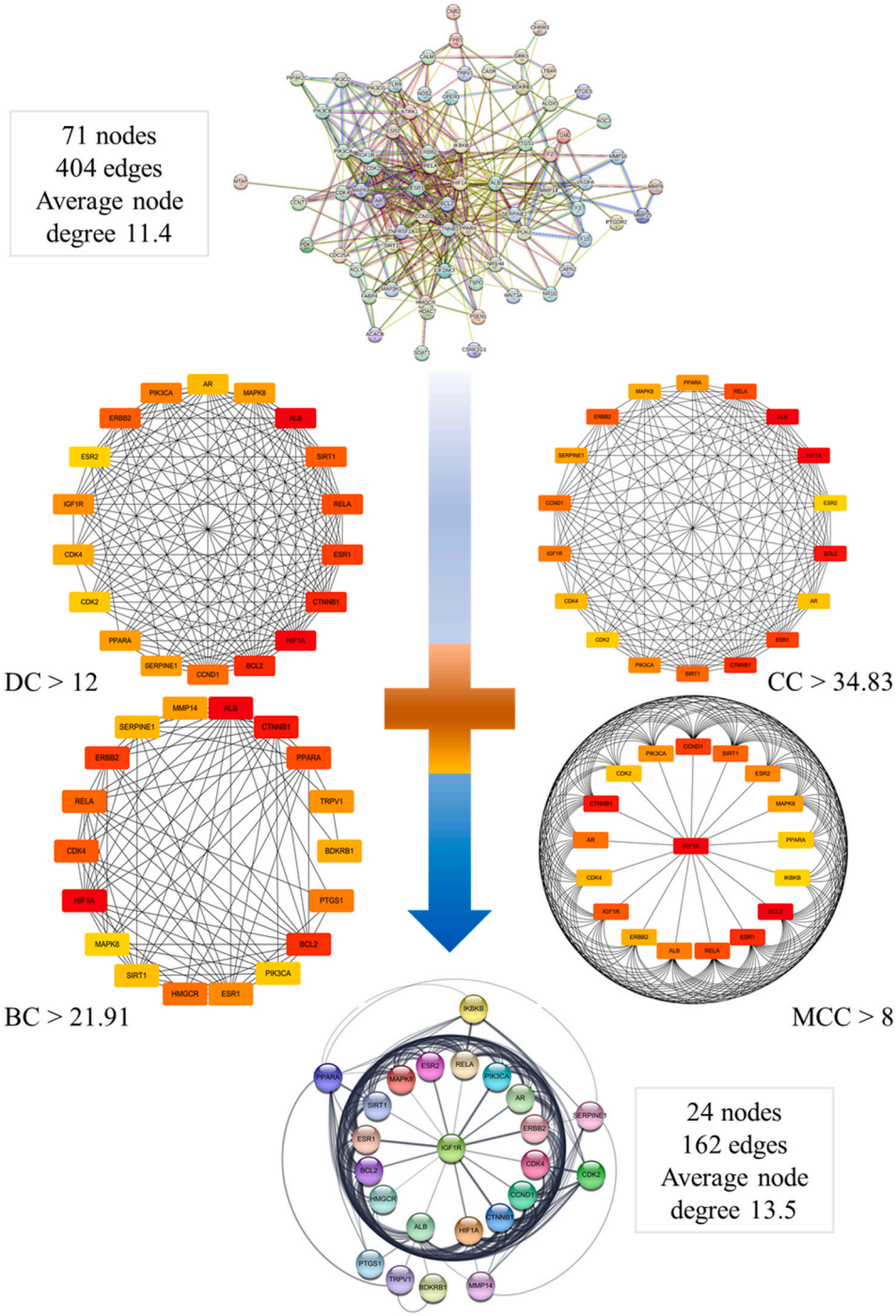

Fig. 2. PPI analysis sequence of ARR-target disease genes by DC, CC, BC and MCC. Based on the four-centrality metrics, the figure shows the top 25 % cut-point values.

therapeutic targets for OA in ARR (Fig. 1C).

3.1.3. PPI analysis for common targets

To construct the PPI network model, common targets were imported into the STRING 11.5 platform, with the organism parameter restricted to *Homo sapiens* and a minimum required interaction score set at 0.4. Excluding the targets PNMT, SLC22A6, FTO, SLC18A2, and SLC22A12, which could not form connections, an initial network of 71 nodes and 404 edges was constructed (Fig. 2). The top 25 % centrality values were DC > 12, CC > 34.83, BC 21.92, and MCC>8. After selecting gene targets that met these criteria and excluding duplicates, 24 hub genes were identified. The centralities of the hub genes are shown in Supplementary Material S11.

3.1.4. GO and KEGG enrichment analysis

GO analysis revealed key pharmacodynamic mechanisms of ARR's active constituents. Common targets for GO analysis were imported using the Metascape platform. As a BP, a total of 411 items including response to hormones (GO:0009725), response to mechanical stimulus (GO:0009612), regulation of growth (GO:0040008), negative regulation of apoptotic signaling pathway (GO:2001234), and tube morphogenesis (GO:0035239), were identified (Fig. 3A and B). As a MF, 36 items, including transcription coactivator binding (GO:0001223), protein kinase activity (GO:0004672), estrogen response element binding

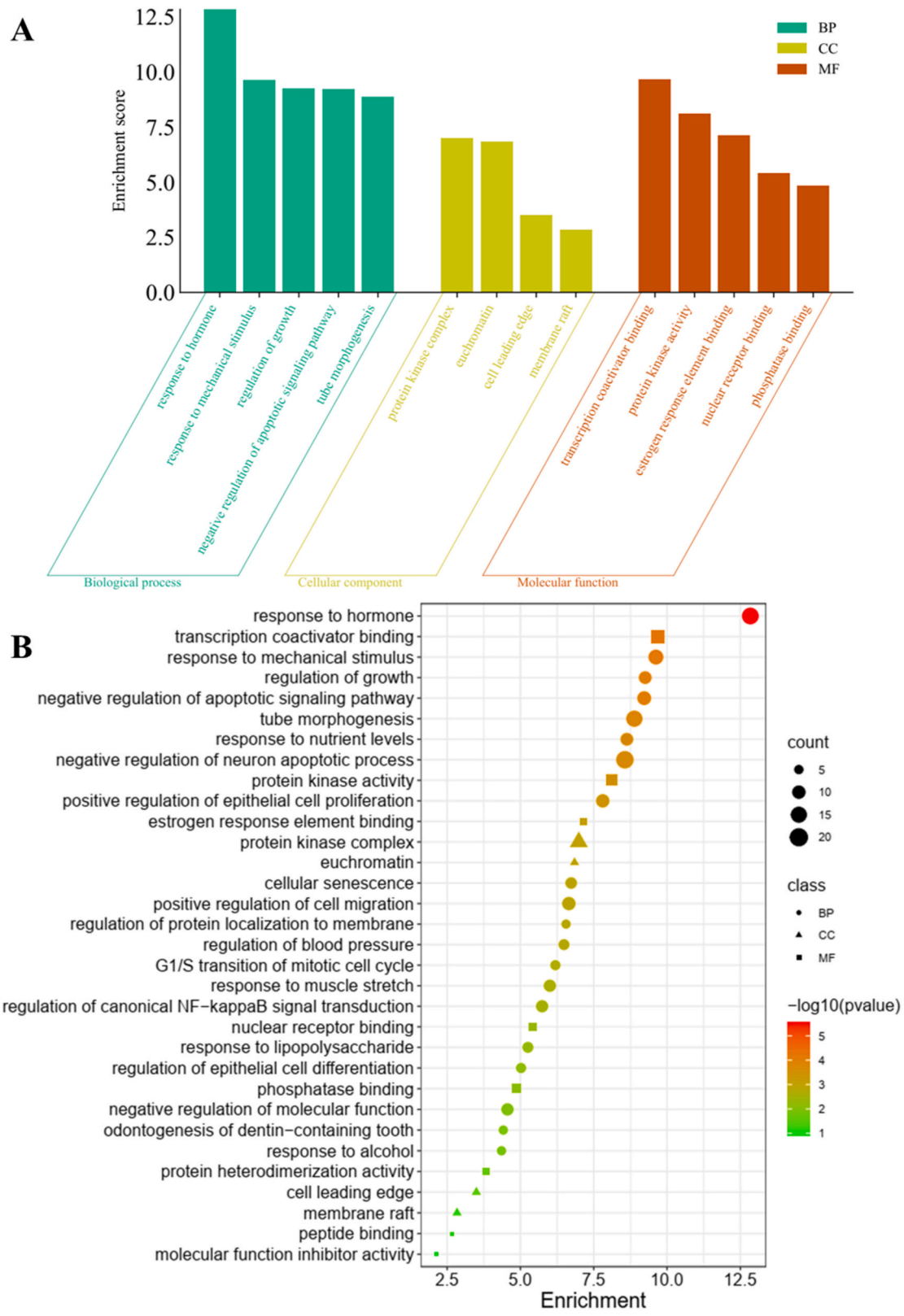

Fig. 3. Functional Enrichment Analysis using GO. **(A)** The five most significantly enriched GO terms within BP, CC, and MF domains. **(B)** Multigroup bubble plot illustrating GO term enrichment across functional domains.

(GO:0034056), nuclear receptor binding (GO:0016922), and phosphatase binding (GO:0019902) were identified (Fig. 3A and B). As a CC, 20 items, including protein kinase complex (GO:1902911), euchromatin (GO:0000791), cell leading edge (GO:0031252), and membrane raft (GO:0045121) were identified (Fig. 3A and B). KEGG pathway enrichment analysis revealed a total of 106 distinct pathways. These results suggest that multiple pharmacological mechanisms of action may converge upon pathways implicated in cancer (hsa05200). Additionally,

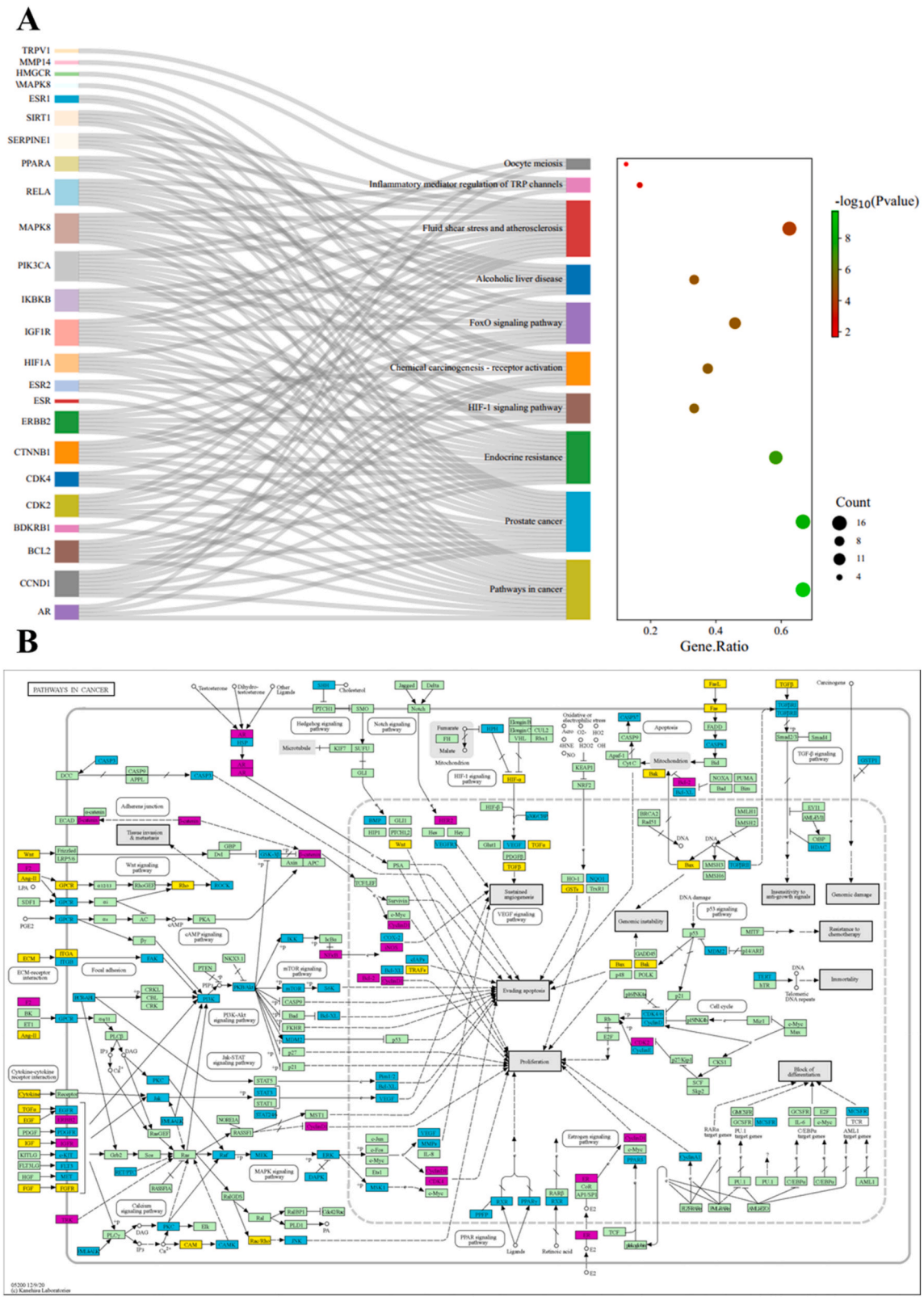

Fig. 4. (A) Visualization of KEGG pathway enrichment analysis using a Sankey diagram and dot plot, highlighting the 10 most significantly enriched pathways. (B) The KEGG mapper was used to color-code pathways in cancer. Color-coded nodes represent the following categories: magenta for ARR elements contributing to osteoarthritis alleviation, cyan for ARR targets not pertinent to OA treatment, and yellow for supplementary OA-related targets. (For interpretation of the references to color in this figure legend, the reader is referred to the Web version of this article.)

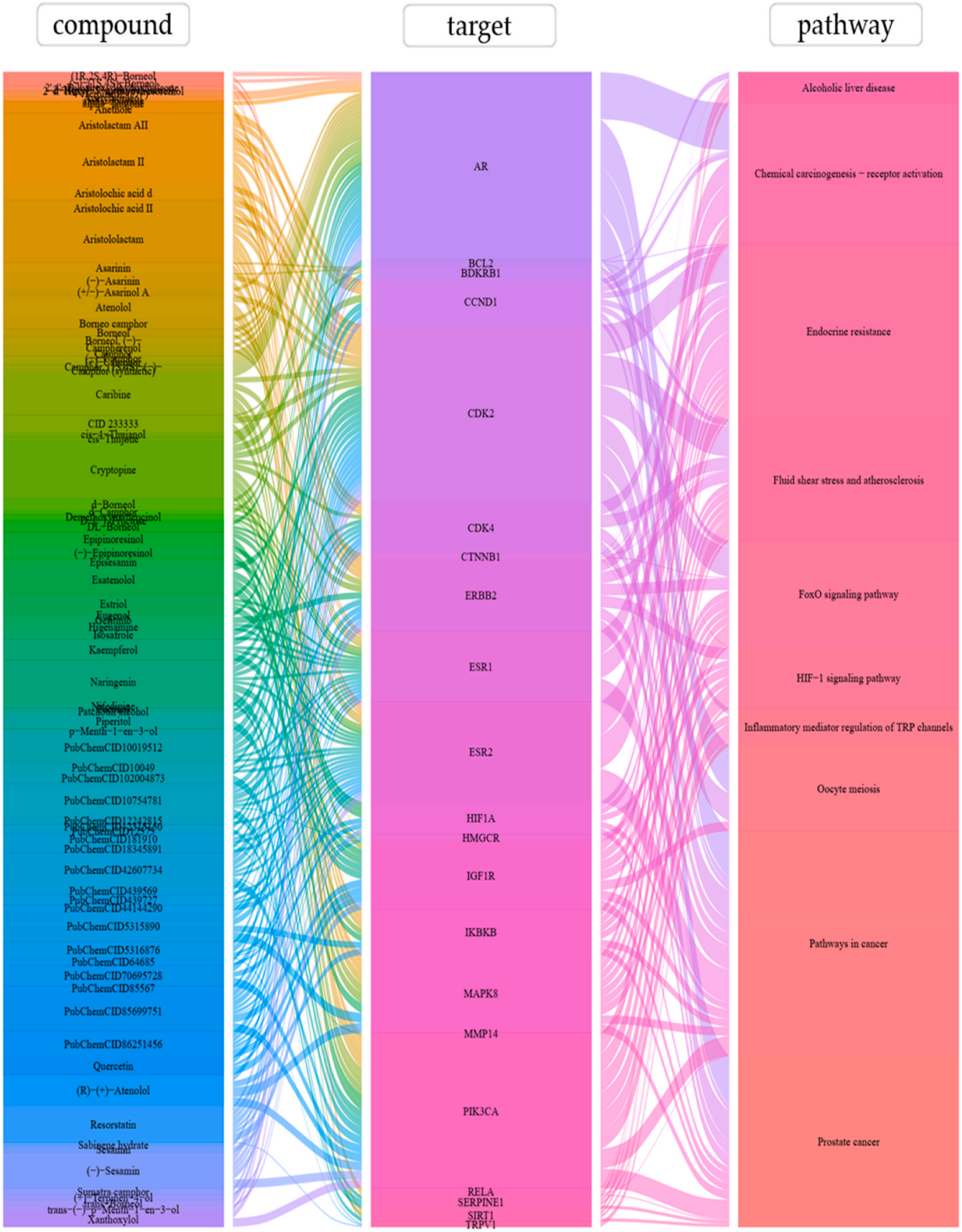

Fig. 5. Alluvial plot showing the compound–target-pathway network for the therapeutic mechanism of target disease from ARR.

Prostate cancer, endocrine resistance, the HIF-1 signaling pathway, chemical carcinogenesis, receptor activation, the FoxO signaling pathway, alcoholic liver disease, fluid shear stress, vatherosclerosis, inflammatory mediator regulation of TRP channels, and oocyte meiosis were important signaling centers of the mechanism (Fig. 4A and B).

3.1.5. Development of a C-T-P network to elucidate the multi-mechanistic action of ARR in OA

To visually represent the interactions between ARR's compounds, their targets, and relevant pathways in OA, we employed an alluvial diagram, a network visualization method. As illustrated in Fig. 5, this

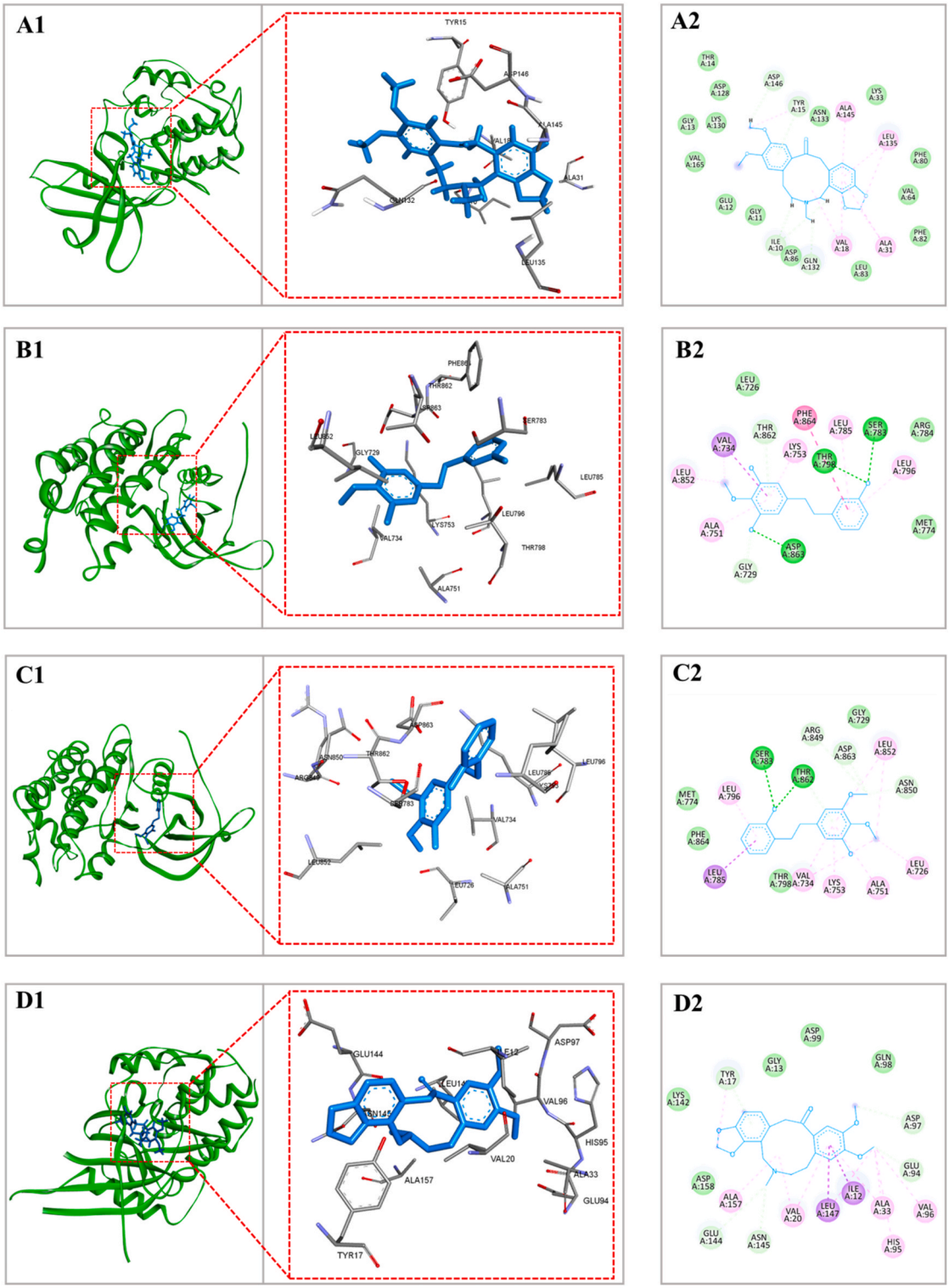

Fig. 6. Docking patterns of hub gene targets and core compounds. (A1) Cryptopine – CCND1 (−8.9 kmol/cal); (B1) 5-[2-(2-Hydroxyphenyl)ethyl]-2,3-dimethoxy-phenol – ERBB2 (−8.9 kmol/cal); (C1) 5-[2-(3-Hydroxyphenyl)ethyl]-2-methoxybenzene-1,3-diol (−9.4 kmol/cal); (D1) Cryptopine – CDK4 (−9.3 kmol/cal); (E1) 5-[2-(2-Hydroxyphenyl)ethyl]-2,3-dimethoxy-phenol – SIRT1 (−9 kmol/cal); (F1) 5-[2-(3-Hydroxyphenyl)ethyl]-2-methoxybenzene-1,3-diol – SIRT1 (−9.1 kmol/cal); (G1) Naringenin – SIRT1 (−9.4 kmol/cal); (H1) Naringenin - MMP14 (−8.8 kmol/cal); (A2), (B2), (C2), (D2), (E2), (F2), (G2), and (H2): 2D representation of bond, respectively. In the 2D representation, van der Waals interactions (bright green) are represented by spoked lines. The dashed lines represent non-polar/polar receptor-ligand interactions such as π–σ interactions (purple/violet), alkyl (light pink), π–π T-shaped (pink), and π–sulfur (gold), conventional hydrogen bonds (solid green) and π−donor hydrogen bonds (green-pastel); (I) Net heatmap of molecular docking results. The x-axis of this heatmap represents the key compounds in ARR and the y-axis represents the primary targets for OA treatment. (For interpretation of the references to color in this figure legend, the reader is referred to the Web version of this article.)

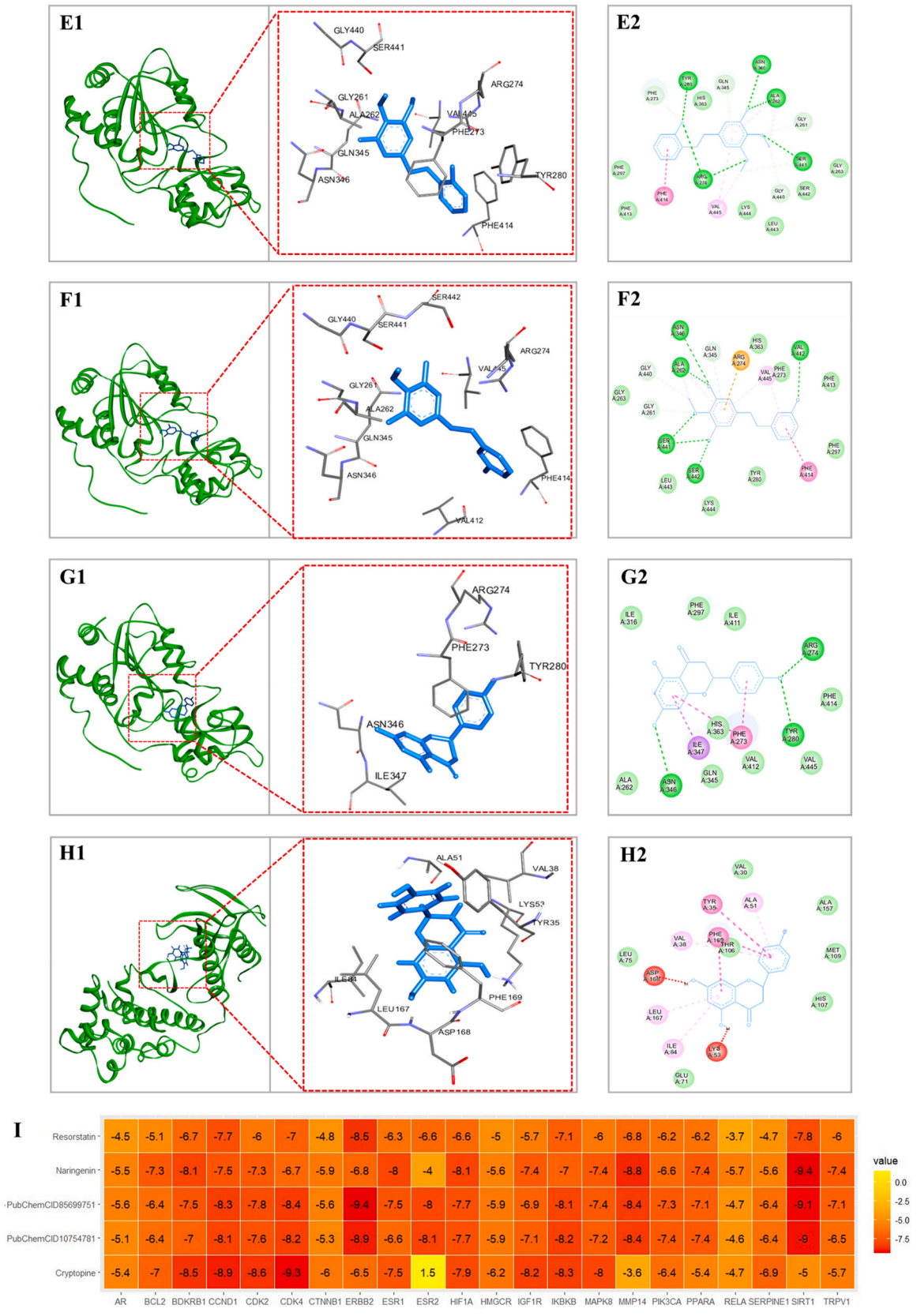

Fig. 6. (*continued*).

network comprised 117 nodes and 335 edges. The nodes consisted of 85 compounds, 22 targets, and 10 pathways. In the network analysis, the core compounds that showed more than three times the median value of degree centrality were, cryptopine, 5-[2-(2-Hydroxyphenyl)ethyl]-2,3-dimethoxy-phenol,5-[2-(3-Hydroxyphenyl)ethyl]-2-methoxybenzene-1,3-diol, Naringenin, and Resorstatin, with centralities of 10, 9, 9, 9, and

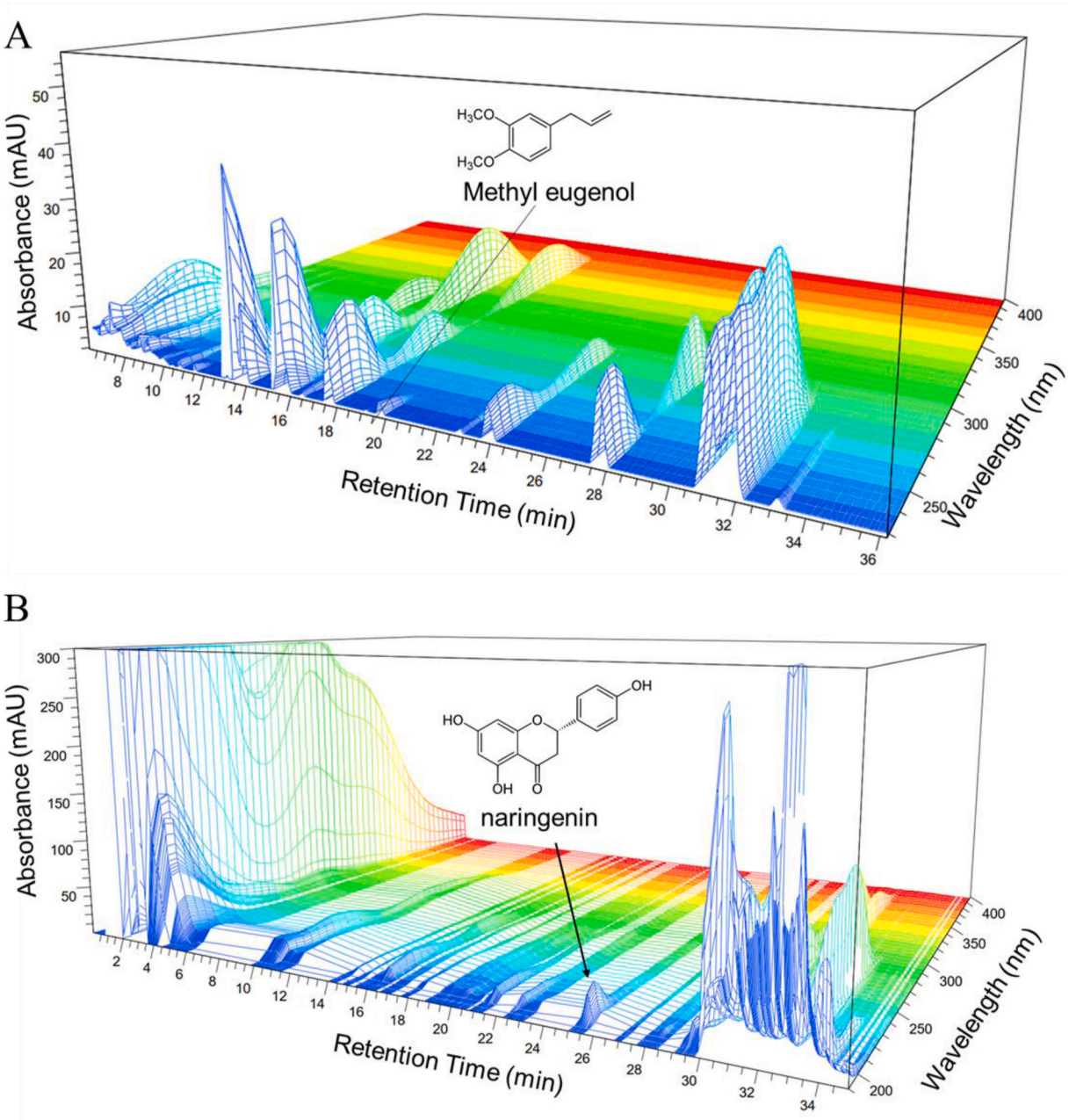

Fig. 7. Analysis using HPLC of the ARR (A) at 230 nm: methyl eugenol Retention time = 19.584 min and (B) at 280 nm naringenin Retention time = 25.285 min. The x-axis represents the retention time; the y-axis means the absorbance unit. A C18 column was utilized for chromatic separation. ARR: *Asarum heterotropoides* F. Schmidt, HPLC: high-performance liquid chromatography chromatogram.

9, respectively. Within the network of therapeutic targets, AR, ESR2, CDK2, PIK3CA, and ESR1 emerged as key nodes, exhibiting notably high centrality scores of 48, 34, 34, 26, and 25, respectively. Pathway in cancer (hsa05200), prostate cancer (hsa05215), and fluid shear stress and atherosclerosis (hsa05418) showed high centrality values of 16, 16, and 15, respectively.

3.1.6. Molecular docking

In order to evaluate the binding energies of five components of ARR (Cryptopine, 5-[2-(2-hydroxyphenyl)ethyl]-2,3-dimethoxy-phenol, 5-[2-(3-hydroxyphenyl)ethyl]-2-methoxybenzene-1,3-diol, Naringenin and Resorstatin), 22 target genes (AR, CCND1, CDK2, PIK3CA, ERBB2, MAPK8, CDK4, IGF1R, IKBKB, HIF1A, BDKRB1, HMGCR, RELA, SERPINE1, SIRT1, CTNNB1, BCL2, TRPV1, PPARA, MMP14, ESR1 and ESR2) were selected for molecular docking studies (Fig. 6A–I). The protein target and ligand have a stronger affinity and a more stable conformation when the binding energy is lower. Acceptable binding activity between the ligand and the receptor should be less than −5 kcal/mol. In our study, molecular docking revealed that most of these binding energies were less than −8 kcal/mol indicating the strong affinities of the compounds for the target protein. The component 5-[2-(3-hydroxyphenyl)ethyl]-2-methoxybenzene-1,3-diol showed maximum

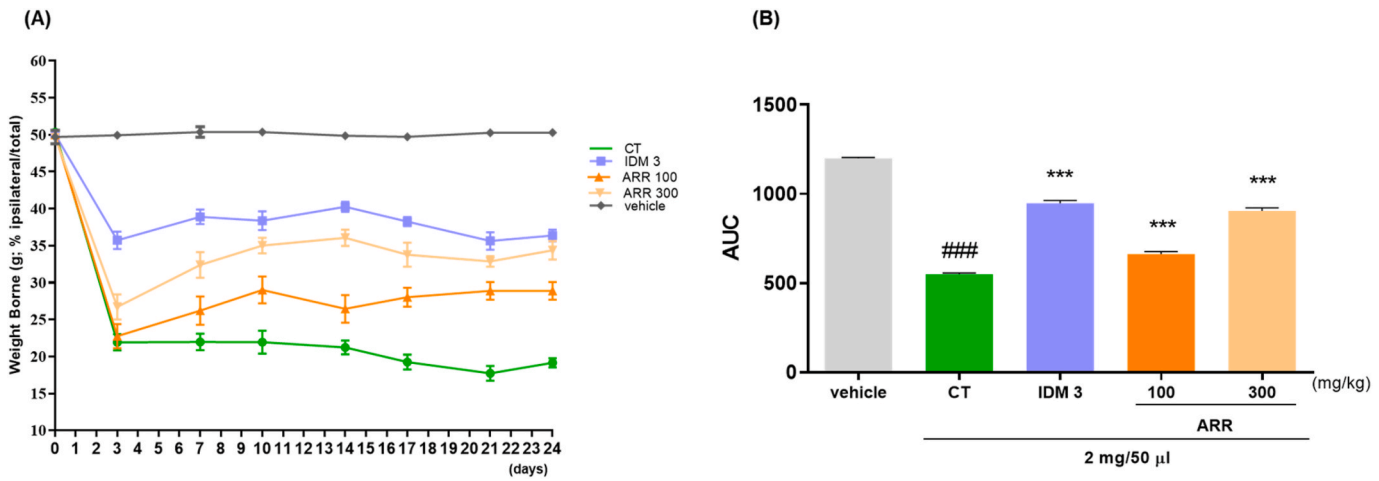

Fig. 8. To evaluate the impact of ARR on enhancing hindlimb weight-bearing capacity in rats with induced OA, (A) measurement of weight-bearing in the ARR 100 and 300 treatment groups and IDM 3 treatment group during 0–24 days and (B) AUC was analyzed with incapacitance tester. ###p < 0.001 vs. vehicle, ***p < 0.001 vs. CT by a 1-way analysis of variance, Dunnett's test. ARR: *Asarum heterotropoides* F.Schmidt, AUC: area under the curve, CT: control, IDM 3: 3 mg/kg of indomethacin. MIA: monosodium-iodoacetate.

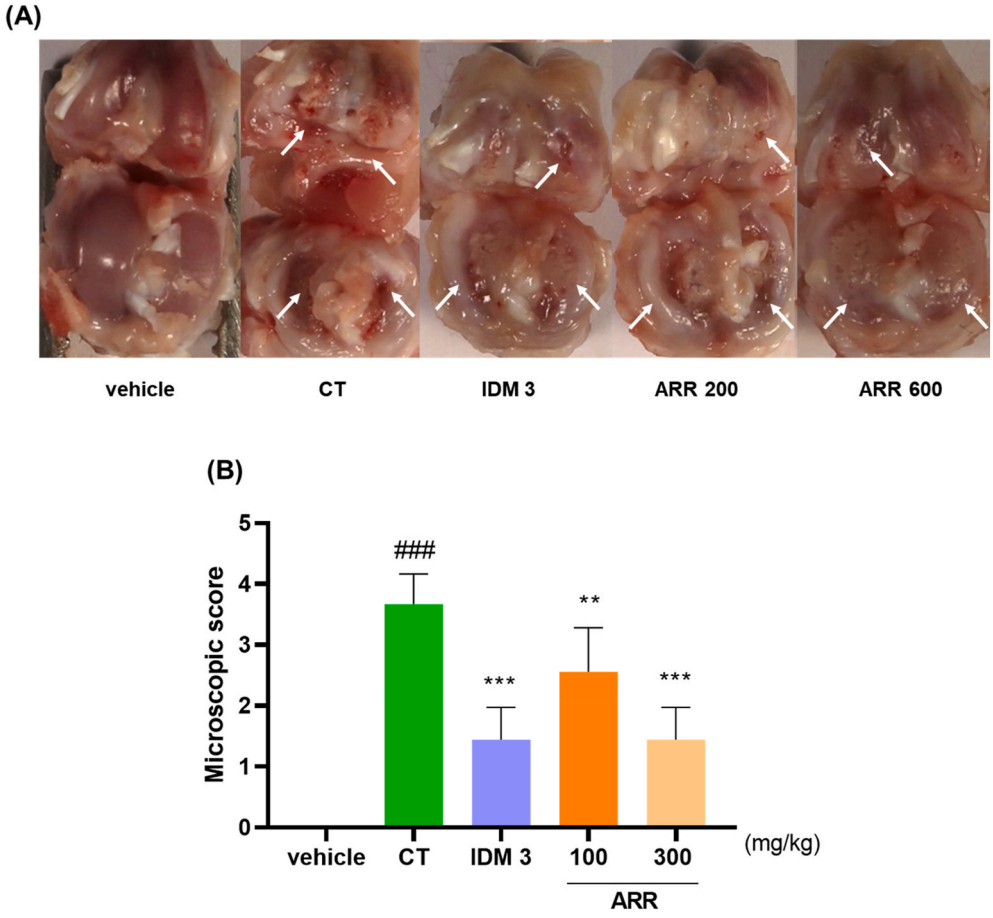

Fig. 9. Photographs of the cartilage of OA induced rats by MIA. IDM 3 and ARR were administered to MIA rats. ###p < 0.001 vs. vehicle, **p < 0.01 vs. CT, ***p < 0.001 vs. CT by a 1-way analysis of variance, Dunnett's test. ARR: *Asarum heterotropoides* F.Schmidt, CT: control, IDM 3: 3 mg/kg of indomethacin. MIA: monosodium-iodoacetate.

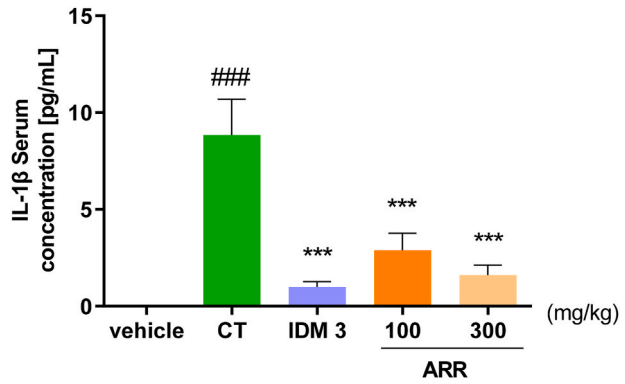

Fig. 10. Analysis of IL-1β in serum. Rats were administered with IDM 3 and ARR during 0–24 days. ###p < 0.001 vs. vehicle, ***p < 0.001 vs. CT by 1-way ANOVA and, Dunnett's test. ARR: *Asarum heterotropoides* F.Schmidt, CT: control, IDM 3: 3 mg/kg of indomethacin. MIA: monosodium-iodoacetate.

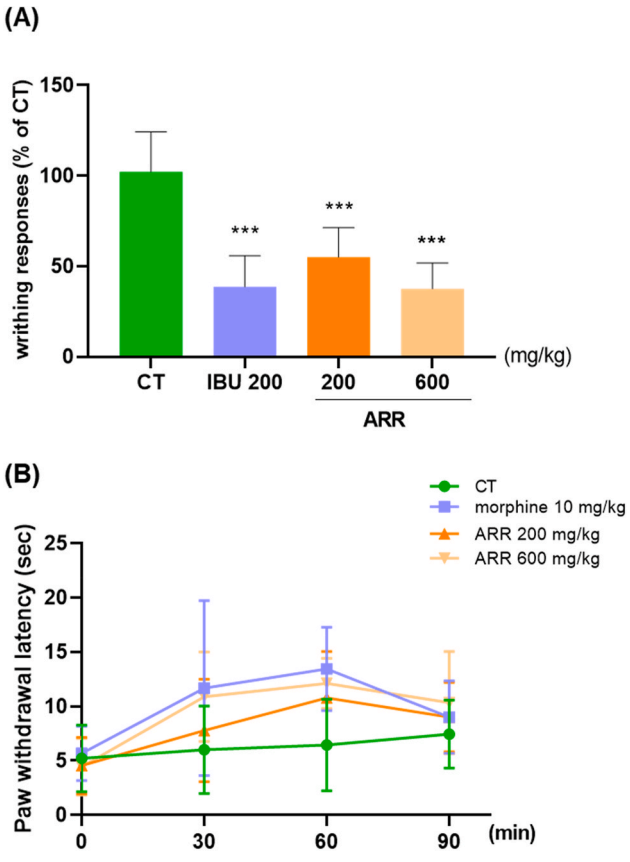

Fig. 11. Effect on analgesic responses using acetic acid induced writhing responses and hot plate test. (A) Thirty minutes after oral administration of IBU 200 and ARR 200 and ARR 600, all groups received an intraperitoneal injection of 0.7 % acetic acid 10 min before recording. The writhes number recorded during 10 min in each group. (B) Hot plate responses recorded with paw withdrawal latency; ***p < 0.001 vs. CT by 1-way ANOVA, Dunnett's test. ARR: *Asarum heterotropoides* F.Schmidt, CT: control, IBU 200: 200 mg/kg of ibuprofen.

binding energy affinities of −9.4 kcal/mol with ERBB2. The highest binding energies were exhibited by the combination of Naringenin with SIRT1 and MMP14 with binding energy values of −9.4 and −8.9 kcal/mol respectively. Interestingly, cryptopine exhibited stronger binding energy values of −8.9, −8.6, −9.3, −8.5 kcal/mol with CCND1, CDK2, CDK4 and BDKRB1 respectively. These higher binding affinities of the ARR components to multiple targets indicate their potential use in the treatment and management of inflammatory pathologies of arthritis (Fig. 6 I).

3.2. HPLC analysis

Methyl eugenol and naringenin were identified in ARR using HPLC-UV. The methyl eugenol and naringenin content in the ARR was 0.2193 and 4.977 mg/g. The chemical structures of the identified components, along with the corresponding HPLC chromatogram, are shown in Fig. 7A and B.

3.3. Evaluation analgesic effects by OA induced models

To assess improvements in OA-induced pain, discomfort and analgesic effects were measured based on weight distribution between the hind legs. The WBR of the right and left limbs were monitored during 0–24 days. As illustrated in Fig. 8, the CT group exhibited a notable decline in WBR after 10 days, followed by a response pattern comparable to IDM 3, with ARR 300 demonstrating the most pronounced effect.

3.4. Assessment of cartilage degradation

Joint cartilage from the OA model was collected and examined after 24 days. The administration of ARR effectively mitigated cartilage damage by MIA solution. As depicted in Fig. 9A, vehicle group appeared smooth and glossy, whereas the CT group exhibited a rough, dull surface with visible damage in certain areas. Evaluated from macroscopic score, rats administrated with ARR and IDM 3 identified notable improvements in cartilage integrity (Fig. 9B). Specifically, damaged cartilage regions showed a comparable level of repair in both the ARR and IDM 3 groups.

3.5. Pro-inflammatory cytokine level on serum of the MIA rats

The IL-1β level in the serum of OA model were analyzed each group. ARR group indicated a significant reduced the level of IL-1β in serum compared with CT in the dose dependent. ARR 300 reduced the IL-1β levels similar to those of IDM 3 rats (Fig. 10).

3.6. Analgesic effects on the pain induced animal models

To assess pain relief, the analgesic effects of ARR were assessed through the writhe's response and the hot plate test. In the writhing test, mice injected acetic acid exhibited an average writhing count of 100 in the CT group after 10 min. Comparatively, the IBU 200 recorded the average of 38.73, while the ARR 600 recorded 37.53, suggesting that ARR 600 identified similar with IBU 200 (Fig. 11A). The hot plate test measured the pain response at 30, 60 and 90 min after sample treatment. Morphine, ARR 200, and ARR 600 analyzed a significant difference at 30 and 60 min, compared with the CT group, with ARR 600 indicated the significant difference at 90 min. In this study, morphine had the greatest analgesic effect 60 min after administration, and ARR 600 had the greatest analgesic effect 90 min after administration. The paw withdrawal latency after 90 min at an ARR of 600 was 10.33 s, whereas that of morphine was 9 s, indicating a more effective analgesic effect (Fig. 11B).

3.7. Cell toxicity, nitric oxide and SOD expression level on the RAW264.7 cells

To evaluate the toxicity of ARR, RAW264.7 cells were incubated with ARR and cytotoxicity was assessed using the MTT assay. ARR exhibited no cytotoxic effects in the RAW264.7 cells (Fig. 12A). To investigate the anti-inflammatory properties, RAW264.7 cells were activated by LPS

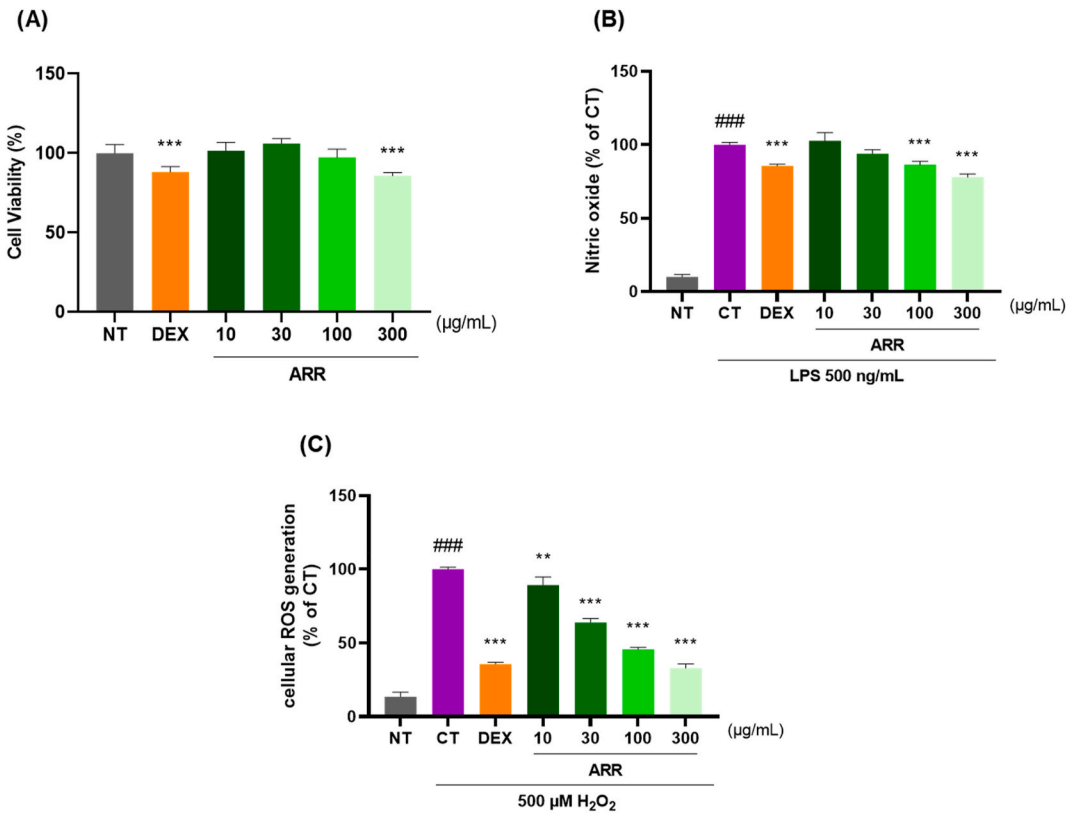

Fig. 12. Effects of ARR on RAW264.7 (A) cell toxicity, (B) LPS-stimulated NO production, and (C) H2O2-activated SOD generation. ###p < 0.001 vs. NT, **p < 0.01 vs. CT, ***p < 0.001 vs. CT by 1-way ANOVA, Dunnett's test. ARR: *Asarum heterotropoides* F.Schmidt, CT: control, DEX: dexamethasone, LPS: lipopolysaccharide, NT: non-treated.

and subsequently incubated for NO analysis. ARR significantly reduced LPS-induced NO production, with the ARR 300 group showing a decrease in NO levels compared to the CT group (Fig. 12B). Additionally, the antioxidant effects of ARR were evaluated by measuring SOD levels in RAW264.7 cells. ARR reduced H_2O_2-induced SOD production dose dependently, further indicating its potential antioxidant properties (Fig. 12C).

3.8. Effects on the anti-inflammatory activity in RAW264.7 cells

The anti-inflammatory activity in the ARR were indicated the LPS-activated RAW264.7 cells. Fig. 13A–T shown that ARR and DEX 1 decreased the levels of TNF-α, COX-2, Ptger2, IL-1β, IL-6, NOS2, MMPs (−1, −3, −8, and −13), CCND1, CDK2, ERRB2, CDK4, IKBKB, HIF1A, BDKRB1, SIRT1, MMP14, ESR1, NLRP3, ASC and caspase-1 mRNA expression (Fig. 13A–W). As shown in Fig. 13X, ARR of LPS-treated RAW264.7 cells reduced the cytokines level by Western blot result. ARR decreased the expression of MMP-1, IL-1β, TNF-α, COX-2, CCND1, CDK2, IKBKB, HIF1A, BDKRB1, SIRT1, MAPK8, NLRP3, ASC and caspase-1 compare with CT groups as seen by the Western blot pictures and charts. The anti-inflammatory in the ARR were found to be on par with those of DEX 1 across all cytokines.

3.9. Effects on the anti-inflammatory activity in OA induced rats

The ARR significantly reduced the cytokines level of TNF-α, COX-2, Ptger2, IL-1β, IL-6, NOS2, MMPs (−1, −3, −8 and −13), CCND1, CDK2, ERRB2, CDK4, IKBKB, HIF1A, BDKRB1, SIRT1, MMP14 ESR1, MAPK8, NLRP3, ASC and caspase-1 in joint cartilage, as compared with CT group, according to the record of the mRNA expression levels (Fig. 14A–X). The down-regulating effects of ARR on IL-1β, IL-6, MMP-1, MMP-3, MMP-13, CCND1, CDK2, IKBKB, HIF1A, BDKRB1, SIRT1, MAPK8, NLRP3, ASC and caspase-1 were indicated with Western blot pictures of OA induced rat's cartilage (Fig. 14Y).

3.10. MD simulation analysis of Errb2 with compound 85699751

The RMSD plot provides insights into the overall stability of the Errb2 protein throughout the MD simulation (Fig. 15). The RMSD remains relatively stable within the range of ~0.2–0.35 nm after an initial equilibration phase, indicating that the system reaches structural stability. Minor fluctuations suggest local conformational adjustments, but no significant structural deviations are observed. The radius of gyration (Rg) plot reveals the compactness of the system over time. The Rg fluctuates around 2.0 nm with slight variations, suggesting that the protein maintains its structural integrity without drastic expansion or collapse. These results indicate that the system has reached equilibrium, with no major unfolding events occurring during the simulation. The RMSF analysis highlights regions of high and low flexibility within the protein. Residues at N-terminal and C-terminal regions exhibit the highest fluctuations, with values exceeding 0.6 nm, indicating greater flexibility. Several loop regions also show moderate fluctuations, suggesting their potential involvement in dynamic interactions. However, the structured core of the protein remains stable, with lower RMSF values, reinforcing the idea that the overall protein structure remains intact. The hydrogen bonding plot reveals fluctuations in the number of hydrogen bonds formed between the ligand and receptor over time. Initially, the system exhibits 1–2 hydrogen bonds, which increase to 2–3 in later stages, suggesting stabilization of ligand binding. This trend indicates that the ligand achieves a more stable binding pose as the simulation progresses. Additionally, hydrophobic interactions and salt bridges likely to contribute to ligand stabilization, further reinforcing the ligand's binding affinity for Errb2.

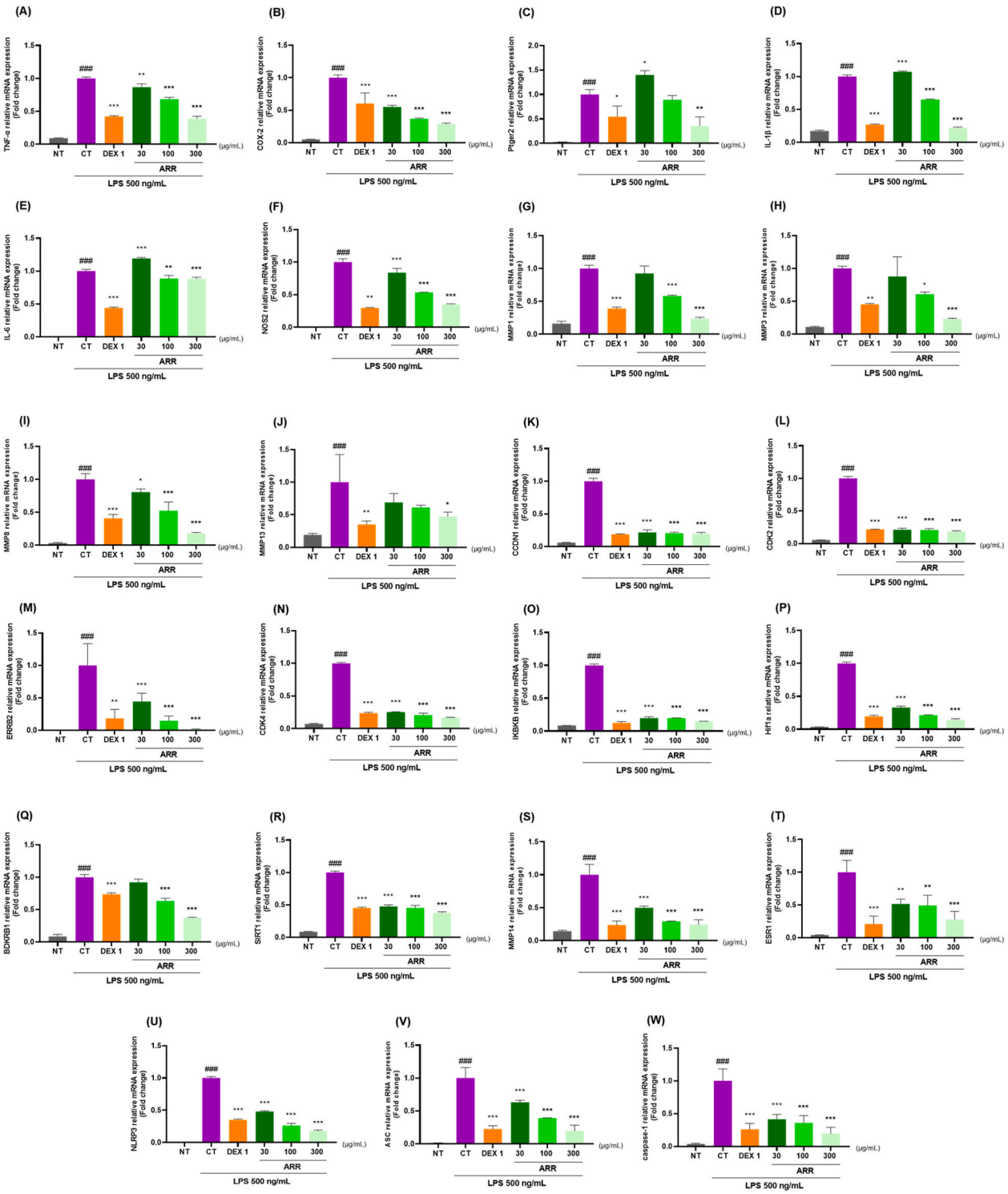

Fig. 13. Cytokine changes in the LPS-induced RAW264.7 cell (A–W) mRNA expression level. TNF-α, COX-2, Ptger2, IL-1β, IL-6, NOS2, MMP-1 MMP-3, MMP-8, MMP-13, CCND1, CDK2, ERRB2, CDK4, IKBKB, HIF1A, BDKRB1, SIRT1, MMP14, ESR1, NLRP3, ASC and caspase-1 and (X) protein expression of MMP-1, IL-1β, TNF-α, COX-2, CCND1, CDK2, IKBKB, HIF1A, BDKRB1, SIRT1, MAPK8, NLRP3, ASC and caspase-1. For a duration of 24 h, the cells were exposed to DEX 1, ARR 30, 100, and 300, and LPS. ###p < 0.001 vs. NT, *p < 0.05 vs. CT, **p < 0.01 vs. CT, ***p < 0.001 vs. CT by a 1-way ANOVA, Dunnett's test. ARR: *Asarum heterotropoides* F.Schmidt, CT: control, IDM 3: indomethacin 3 mg/kg, LPS: lipopolysaccharide, NT: non-treated.

3.11. MD simulation analysis of SIRT1 with compound naringenin

The RMSD plot provides insight into the global stability of the SIRT1 protein throughout the MD simulation (Fig. 16). RMSD increases from ~0.3 to ~0.6 nm within the first 50ns, indicating structural adaptation. Subsequently, RMSD continues fluctuating between 0.6 nm and 0.8 nm, suggesting that while the system remains relatively stable, there are ongoing conformational adjustments. This level of fluctuation suggests moderate flexibility within the system, likely due to the dynamic nature of the ligand binding process. The Rg plot tracks the compactness of the

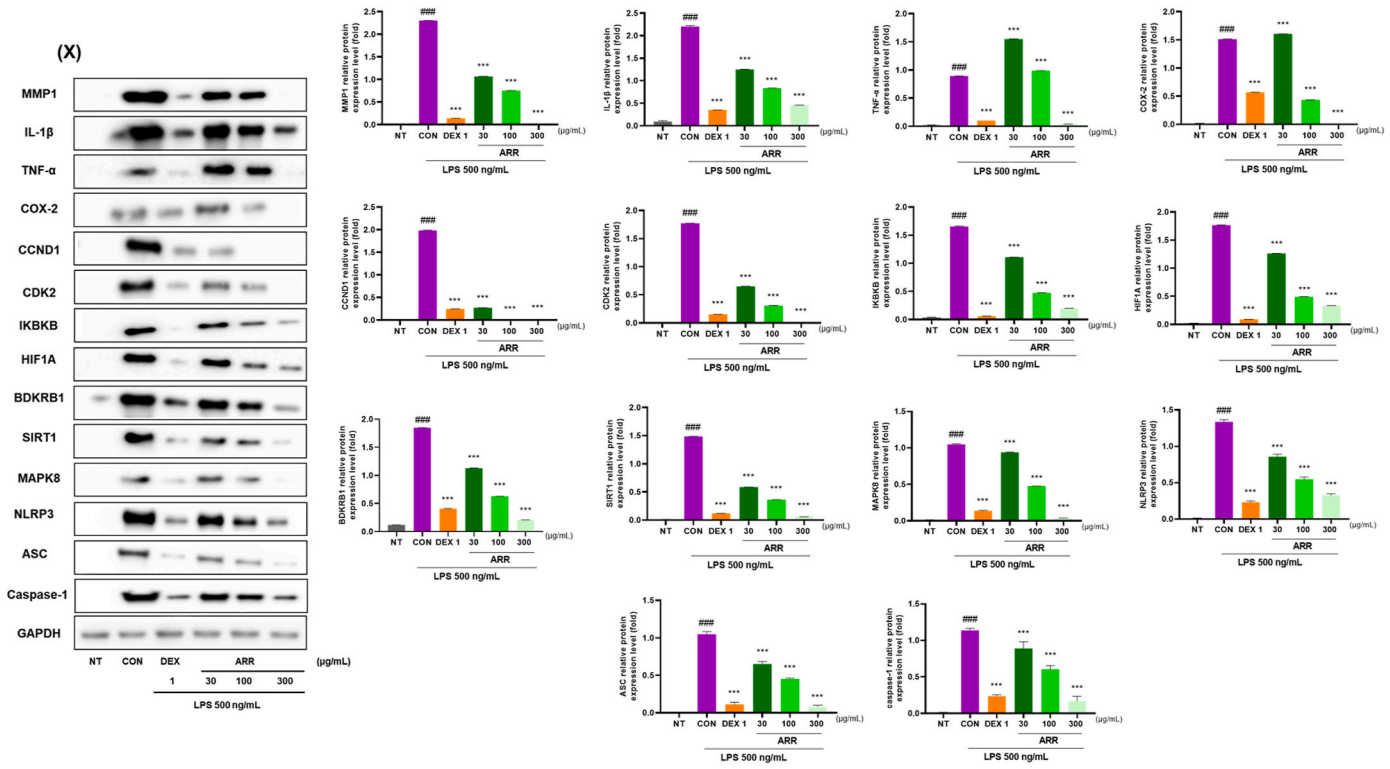

Fig. 13. (*continued*).

protein throughout the trajectory. The values fluctuate between ~2.0 and ~2.15 nm, indicating that the system undergoes slight structural expansion during ligand binding. The minor increase in Rg values after ~100ns suggests a shift in protein conformation, possibly due to ligand-induced rearrangements. However, towards the end of the simulation, Rg values stabilize, suggesting the system reaches equilibrium. The RMSF plot highlights residue-specific flexibility. Most residues exhibit moderate fluctuations (~0.2–0.5 nm), while specific regions, particularly near residue ~500, show significantly higher fluctuations (>2.0 nm). This high flexibility at the C-terminal region suggests that it is highly dynamic and possibly involved in the interactions or conformational changes. Loop regions also exhibit noticeable fluctuations, which may contribute to ligand accommodation. The hydrogen bond analysis provides insights into ligand stabilization within the binding pocket. The number of hydrogen bonds fluctuates between 1 and 3 throughout the simulation, indicating dynamic ligand-receptor interactions. Peaks in hydrogen bonding around 100ns and 150ns suggest transient stabilization events, which may be critical for ligand affinity. In addition to hydrogen bonds, hydrophobic interactions and possible salt bridges contribute to ligand binding, further stabilizing the complex.

4. Discussion

Leveraging an integrative network analysis framework incorporating functional genomic data, this study aimed to predict the primary bioactive compounds and cognate gene targets through which ARR mediates its therapeutic action in mitigating OA inflammatory pathology(Wang et al., 2024). Molecular docking was performed to validate these predictions. The five major compounds investigated in this study were cryptopine, 5-[2-(2-Hydroxyphenyl)ethyl]-2,3-dimethoxy-phenol, 5-[2-(3-Hydroxyphenyl)ethyl]-2-methoxybenzene-1,3-diol, Naringenin, and Resorstatin. Molecular docking analyses suggested that these key compounds exhibited favorable overall binding affinities for multiple gene targets. These findings suggest that ARR may inhibit multiple inflammatory pathways in OA. Therefore, we conducted further in vivo and in vitro studies. ARR demonstrated significant mRNA expression inhibition-based anti-inflammatory effects on a wide range of markers in RAW264.7, and exhibited similar trends in its ability to inhibit cytokines in joint cartilage. Beyond its network-predicted mechanisms, ARR also delivers tangible therapeutic benefits in OA, including analgesia, functional restoration, and chondral preservation, consistently demonstrated across diverse in vivo models. To our knowledge, this is the first study to combine network pharmacology with experimental validation in the context of osteoarthritis treatment. By integrating in silico predictions with in vitro and in vivo experiments, we successfully demonstrated ARR's multi-targeted anti-inflammatory mechanisms and therapeutic effects, highlighting the value of this novel methodology for drug discovery.

These findings suggest ARR alleviates OA pathology by inhibiting multiple inflammatory targets. Naringenin, a key predicted compound and extensively studied flavonoid, demonstrates broad anti-inflammatory activity by modulating pro-inflammatory mediators (Cai et al., 2023). Specifically, naringenin inhibited joint inflammation in a rat CIA model by suppressing $CD4^+$ T lymphocyte polarization and mitochondrial redistribution (Jiang et al., 2022) and mitigated RA inflammation by modulating T helper/regulatory T cell polarization (Wang et al., 2018). Molecular docking predicted strong naringenin binding affinities for MMP14 and SIRT1. MMP14 inhibition may impede cartilage destruction in RA and OA (Kaneko et al., 2016; Yamamoto et al., 2017), while SIRT1 promotes ECM synthesis and cell survival, representing a therapeutic target for reversing OA-related deterioration (Ansari et al., 2024; Dvir-Ginzberg and Steinmeyer, 2013). Multiple reports support naringenin's effectiveness against multifaceted OA pathology (Pan et al., 2022; Y. Wang et al., 2023). Naringenin's pharmacological properties likely contribute significantly to the observed anti-OA effects of ARR. However, molecular docking predicted strong binding affinities for other key compounds to multiple targets, indicating ARR's broad in vitro modulatory effects likely stem from more than a single compound. Future studies should investigate the individual activities and interactions of other key compounds to fully elucidate

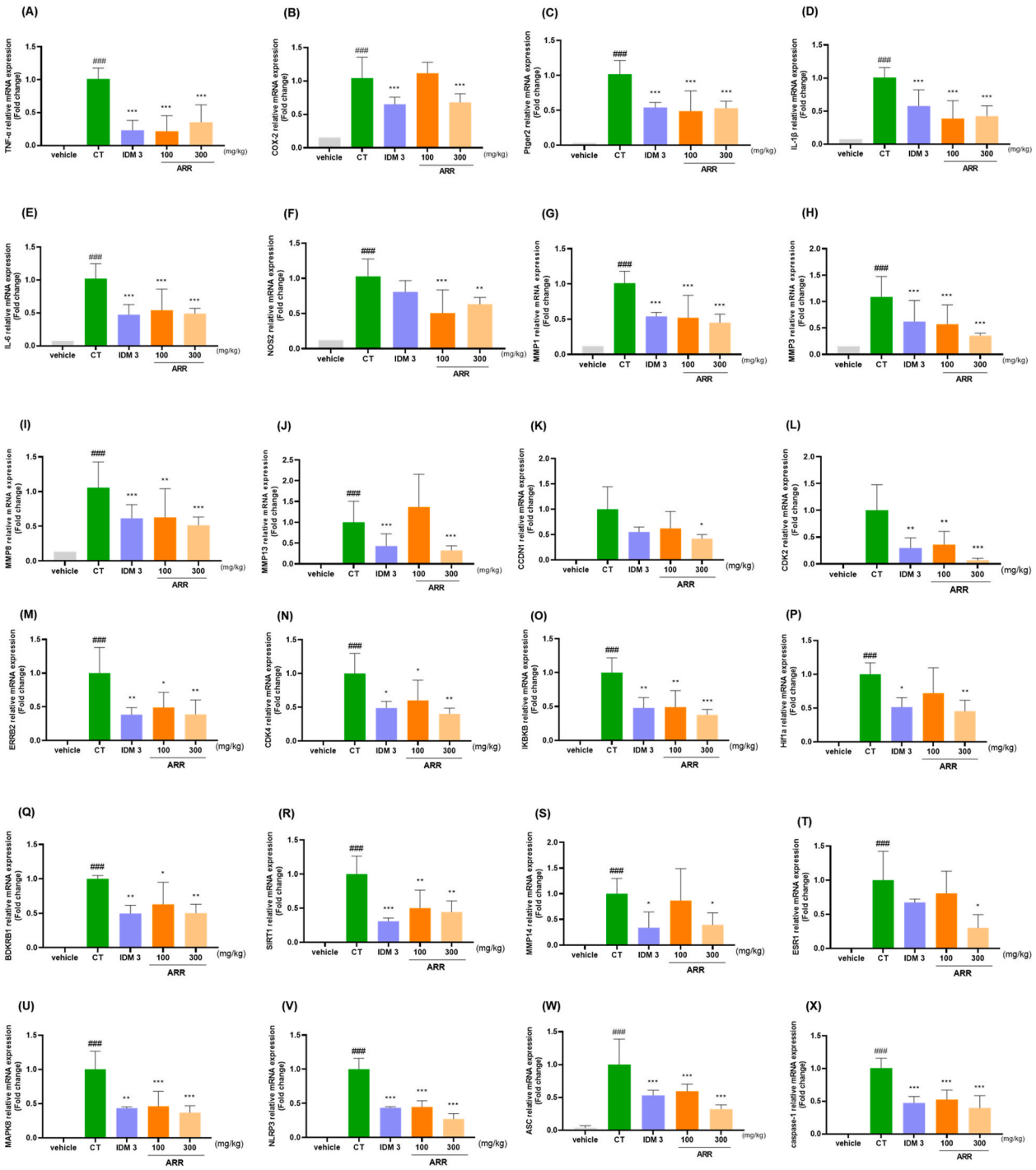

Fig. 14. Cytokine levels decreased at the joint cartilage following ARR treatment. (A–X) Using qRT-PCR, the mRNA expression of TNF-α, COX-2, Ptger2, IL-1β, IL-6, NOS2, MMP-1, MMP-3, MMP-8, MMP-13, CCND1, CDK2, ERRB2, CDK4, IKBKB, HIF1A, BDKRB1, SIRT1, MMP14 ESR1, MAPK8, NLRP3, ASC and caspase-1 was verified. (Y) Western blotting was evaluated to protein expression level of IL-1β, IL-6, MMP-1, MMP-3, MMP-13, CCND1, CDK2, IKBKB, HIF1A, BDKRB1, SIRT1, MAPK8, NLRP3, ASC and caspase-1. ###$p < 0.001$ vs. vehicle, *$p < 0.05$ vs. CT, **$p < 0.01$ vs. CT, ***$p < 0.001$ vs. CT by one-way ANOVA, Dunnett's test. ARR: *Asarum heterotropoides* F.Schmidt, CT: control, IDM 3: 3 mg/kg of indomethacin.

ARR's multi-component anti-OA effects.

KEGG pathway analysis implicated several signaling pathways in ARR's OA alleviation mechanism, notably "pathways in cancer" and "fluid shear stress." Cancer-related pathways govern processes including invasion, angiogenesis, apoptosis, proliferation, and cytokine interactions. KEGG mapping highlighted numerous targets linked to cell proliferation, considered relevant for inhibiting fibroblast-like synoviocyte (FLS) proliferation in OA. Supporting this, Gadd45β expression promotes FLS inflammation and proliferation in OA rat synovium (Wu et al., 2024). This suggests ARR may delay OA progression by inhibiting FLS proliferation and associated inflammation, partially observed in vivo and in vitro here. This aligns with findings that chondrocytes from end-stage OA synovial fluid exhibit abnormal proliferation and hypertrophy (Housmans et al., 2022). Furthermore,

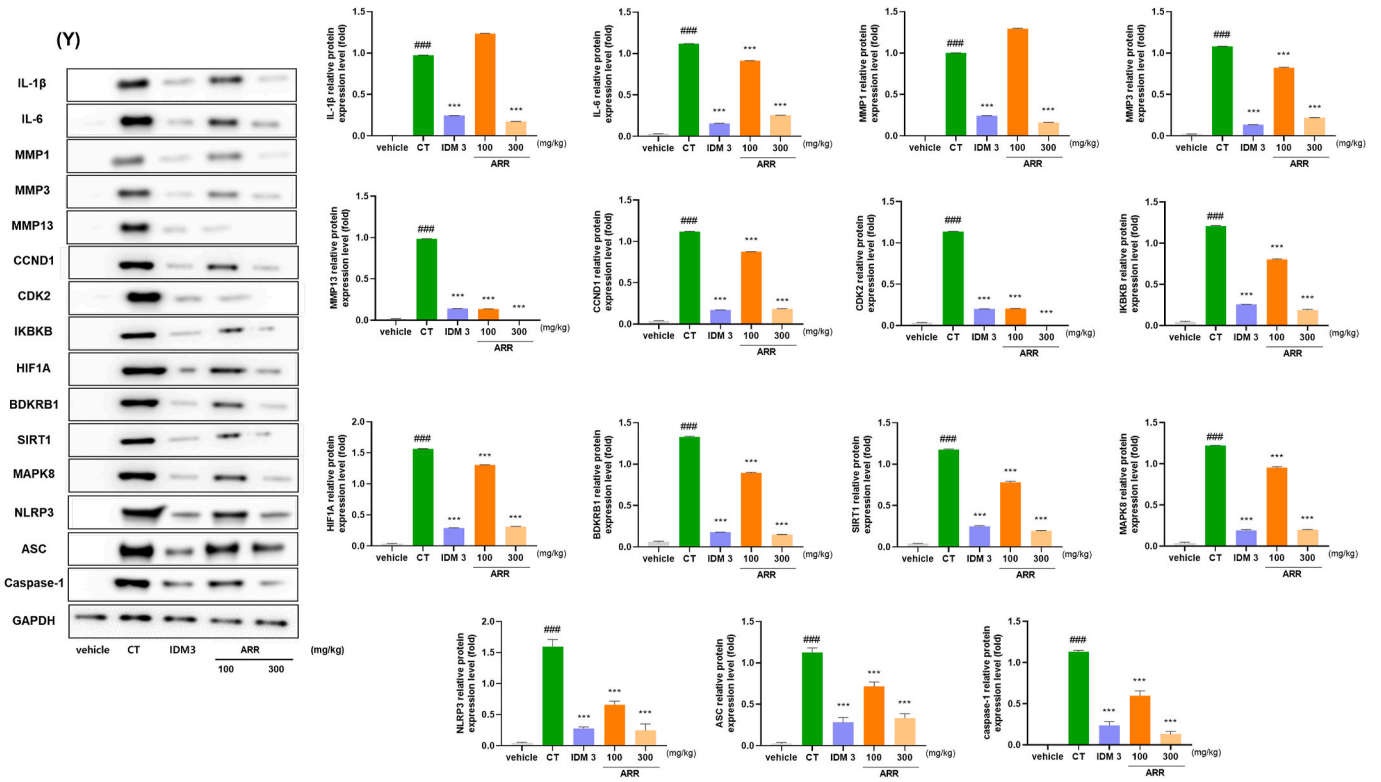

Fig. 14. (*continued*).

fluid shear stress on chondrocytes directly triggers OA pathology, including pro-inflammatory cytokine/MMP release and apoptosis (Wang et al., 2013). High fluid shear stress dysregulates cyclooxygenase-2, increasing prostaglandin E2 in early OA. This helps explain how ARR's anti-inflammatory effects suppress progressive joint destruction in OA, beyond pain relief. Based on prior findings and this study's predictive analyses, ARR was postulated as an efficacious candidate for inhibiting OA progression. These in silico predictions, covering ARR activity against multiple targets and key pathways, were validated in vivo and in vitro.

Our in vitro investigations demonstrated ARR mitigates osteoarthritic joint inflammation via multifaceted actions, showing dose-dependent modulation of MMP-1, MMP-3, MMP-8, MMP-13, IL-1β, IL-6, MAPK8, and CDK2. These findings align with reports of ARR's anti-inflammatory effects in RA models through NF-κB/MAPK inhibition and suppression of TNF-α, IL-1β, and IL-6(Zhang et al., 2014). This broad inflammation inhibition likely underlies the superior analgesic and functional improvements observed in vivo. Persistent OA inflammation sensitizes peripheral/central nerves, causing mechanical allodynia and hyperalgesia (Bjurström et al., 2022; van Helvoort et al., 2021). ARR's potent anti-inflammatory effects target this chronic inflammatory pain mechanism, distinct from acute pain, linking it directly to pain management and functional gains in OA. Furthermore, ARR notably inhibited MMPs (−1, −3, −8, −13) strongly associated with progressive OA cartilage destruction (Grillet et al., 2023). These MMPs significantly contribute to destructive joint pathology; MMP-3 activates other MMPs, while cytokines like IL-1 stimulate MMP-1 and -13 to degrade cartilage collagen. Therefore, MMPs are key therapeutic targets for inhibiting cartilage destruction. Considering the substantial chondroprotective effects observed in vivo (MIA model), ARR emerged as a potential DMOAD candidate due to its broad activity inhibiting pain, functional decline, and progressive joint destruction, warranting further mechanistic investigation.

Overall, The experimental markers identified in this study—including IL-1β, TNF-α, MMPs, CCND1, CDK2, IKBKB, HIF1A, BDKRB1, SIRT1, MAPK8, and NLRP3—primarily function as downstream effectors of the NF-κB/MAPK signaling axis, which orchestrates inflammatory and catabolic processes OA(Jang et al., 2014; P. Wang et al., 2023; Yao et al., 2023). NF-κB activation, driven by cytokines or mechanical stress, transcriptionally upregulates MMPs and cytokines, perpetuating cartilage degradation and synovitis(Gordon et al., 2009; Haseeb et al., 2013; Yao et al., 2023). The suppression of IKBKB and MAPK8 by ARR aligns with their roles in NF-κB/MAPK-mediated MMP-13 induction and chondrocyte apoptosis, while SIRT1 and HIF1A modulation reflects cross-talk between metabolic and inflammatory pathways(Kauppinen et al., 2013; Sabio and Davis, 2014; Zhu et al., 2025). These findings correlate with network pharmacology predictions of ARR targeting "cancer" and "fluid shear stress" pathways, which share molecular nodes such as PI3K-Akt and ERBB2, regulating synovial hyperplasia and mechanotransduction-driven inflammation(Yao et al., 2023). For instance, the predicted "cancer" pathway's emphasis on proliferation aligns with ARR's inhibition of CCND1/CDK2-mediated chondrocyte cycle dysregulation, while "fluid shear stress" mirrors ARR's suppression of MMPs and cytokines induced by mechanical strain. Thus, the network predictions provided a systems-level framework that experimental validation contextualized into OA-specific NF-κB/MAPK-centric mechanisms, demonstrating functional synergy between computational and empirical findings.The anti-inflammatory activity of ARR against numerous targets and its modulation of OA pathological pathways, as elucidated in the preceding discussion, are summarized in Fig. 17.

The MD simulation analysis demonstrates that Errb2 maintains structural stability upon ligand binding, with local conformational changes facilitating ligand accommodation. The flexible regions identified in the RMSF analysis may play a role in ligand-induced adjustments, while the increasing number of hydrogen bonds suggests progressive stabilization of the ligand-receptor interaction. These insights provide valuable information for further optimizing ligand design and improving binding affinity. The MD simulation reveals that SIRT1 undergoes moderate conformational adaptations upon binding

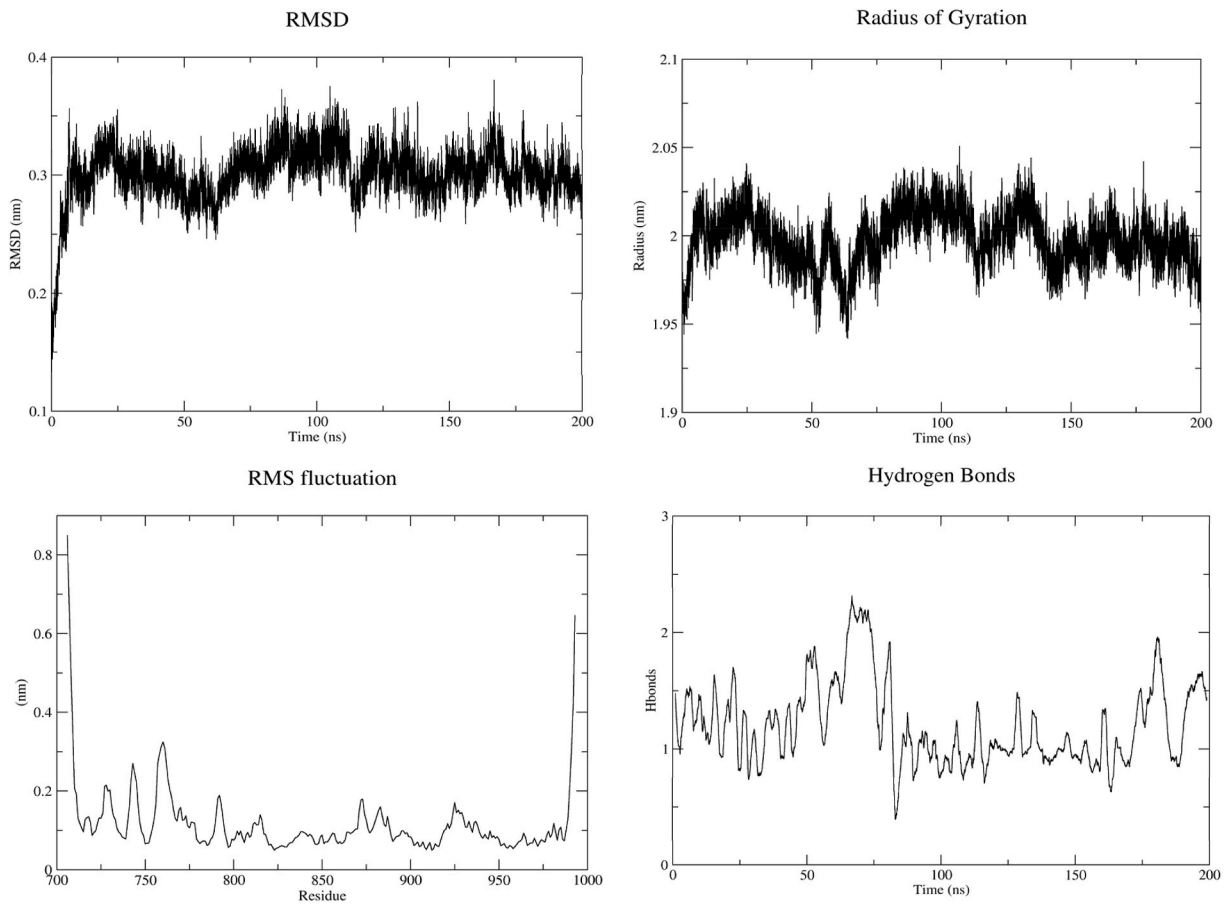

Fig. 15. Molecular Dynamics Simulation of Erbb2-Compound 85699751 Complex (200ns). Root Mean Square Deviation (RMSD) plot demonstrating complex stability with observable conformational fluctuations. Root Mean Square Fluctuation (RMSF) analysis illustrating residue-specific flexibility. Radius of Gyration (Rg) indicating stable global conformation. Hydrogen bond analysis highlighting key protein-ligand interactions throughout the simulation.

Naringenin, with loop regions and the C-terminal domain exhibiting significant flexibility. The system maintains overall stability, and ligand binding is reinforced by hydrogen bonds and hydrophobic interactions. These findings provide valuable insights for further optimizing ligand interactions and enhancing binding affinity for therapeutic targeting of SIRT1.

The results of this study represent the first attempt to determine whether further investigation of ARR as a candidate for DMOAD is warranted. Therefore, this study was exploratory in nature, and the results should not be extrapolated without considering several limitations. First, the data-driven predictions in this study, including network pharmacology and molecular docking, should be viewed as precise hypotheses rather than definitive conclusions. Different predictions can be obtained under different analytical conditions. To address this inherent limitation, we undertook a comprehensive experimental approach encompassing both in vivo and in vitro methodologies. However, we acknowledge that a comprehensive elucidation of the anti-OA mechanisms of ARR and the specific roles of its numerous important components requires several follow-up studies, which are currently being planned. Second, although this study confirmed the inhibition of OA cartilage destruction by ARR, it did not assess its effect on overall joint destruction. A crucial criterion for a DMOAD candidate the ability to inhibit the broad inflammatory pathology of OA and specifically halt or delay progressive joint destruction. Given the broad anti-inflammatory activity of ARR identified in this study, along with its potent inhibitory effects on MMPs, we intend to conduct follow-up studies to ascertain whether ARR can inhibit progressive cartilage destruction and osteoporotic changes over an extended period. Third, because this study was designed as a preliminary screen, the experiments did not specifically validate the predicted anti-inflammatory mechanisms of ARR, including signaling pathways or dose-response relationships. Future studies should include a more specific validation plan to determine the optimal dose and the key pathways of action. Fourth, although the main active components of the ARRs predicted in this study are believed to have contributed significantly to the anti-OA effect, their respective contents could not be confirmed by HPLC because of the challenges in obtaining standards. Future studies may enhance our understanding of the mechanism by verifying the contents of these main active components in specific ARRs and determining the ratio of their contribution to the effect compared with the crude extract. Further analyses designed to systematically address the above limitations will be conducted to further clarify the potential of ARRs with promising anti-OA activities as DMOAD candidates. Finally, although molecular dynamics simulations were conducted to evaluate the predicted ligand–target interactions, direct biophysical binding assays such as SPR or MST were not performed. In future studies, we plan to prioritize these experiments to quantitatively assess the binding affinity and specificity of ARR-derived compounds toward their predicted targets.

5. Conclusion

In summary, this study provides experimental evidence that ARR extract alleviates key pathological features in preclinical models of osteoarthritis. In vivo, ARR administration demonstrated significant analgesic effects, improved functional weight-bearing in OA rats, reduced macroscopic cartilage degradation, and decreased serum IL-1β levels. These beneficial effects were supported by in vitro findings and molecular analyses in OA cartilage, where ARR suppressed the

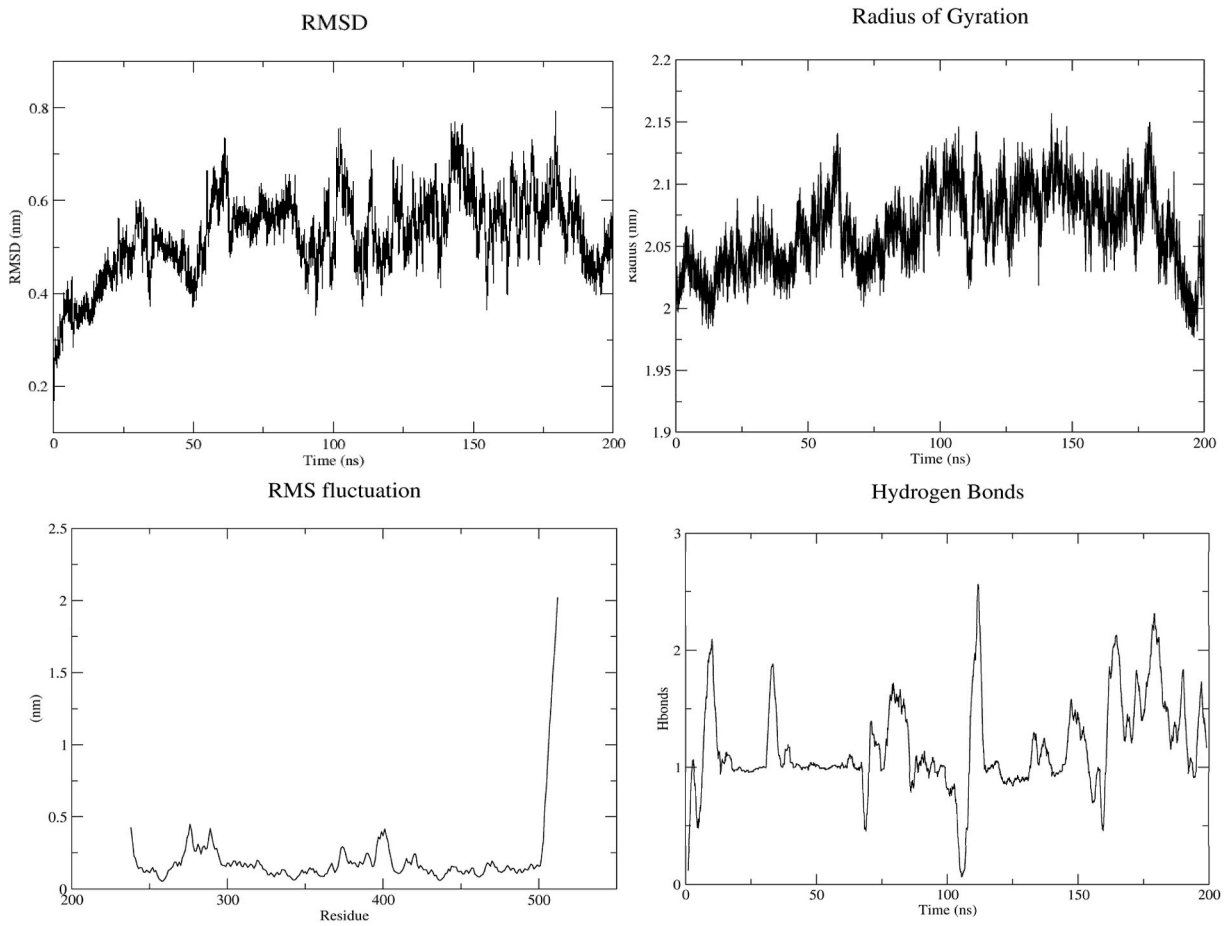

Fig. 16. Molecular Dynamics Simulation of Sirt1 complex with Naringenin RMSD plot (200ns simulation) demonstrating the stability of the Sirt1 (PDB: 4I5I) complex with Naringenin, with observed fluctuations indicating conformational dynamics. RMSF analysis illustrating residue-specific flexibility within the complex. Rg plot, showing the overall conformational stability of the complex. Interfacial hydrogen bond occupancy analysis, revealing stable hydrogen bond formation between Sirt1 and Naringenin throughout the simulation.

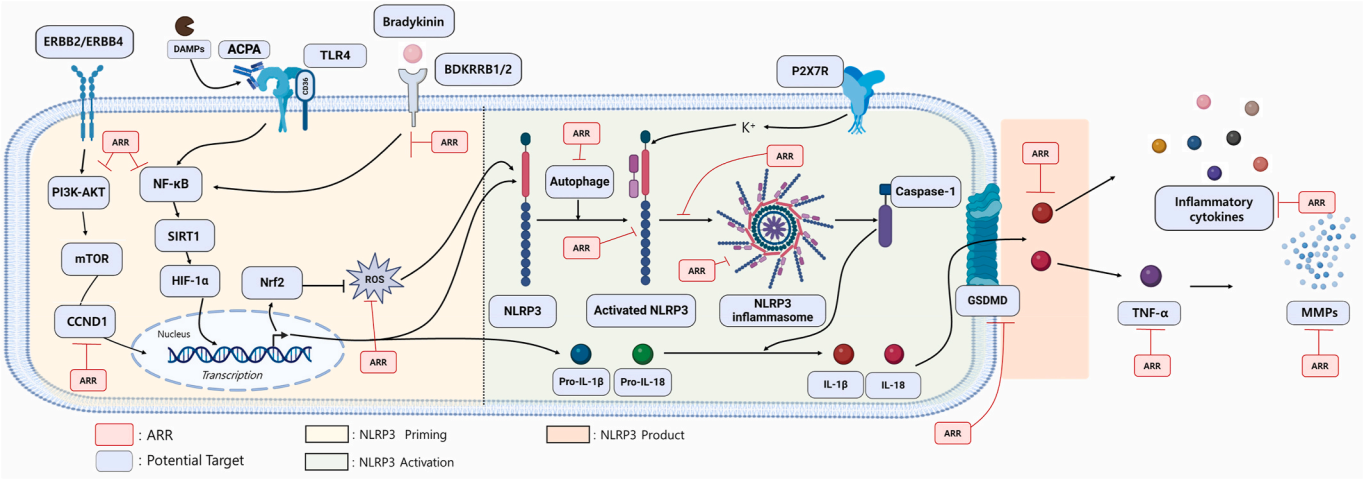

Fig. 17. Multi-target anti-inflammatory mechanism implicated in the OA-alleviating action of ARR, as elucidated in this study.

expression of multiple pro-inflammatory cytokines (including IL-1β, IL-6, TNF-α) and matrix metalloproteinases (MMP-1, -3, -13), crucial mediators of inflammation and cartilage destruction in OA. These observed effects are underpinned by the multi-component, multi-target nature of ARR, as initially suggested by our network pharmacology analysis which identified key potential compounds (cryptopine, Naringenin, etc.) and hub targets (AR, ESRs, PIK3CA, SIRT1, MMP14 etc.) implicated in inflammation and OA progression. The experimentally observed suppression of MMPs and inflammatory cytokines aligns well with these predictions. Furthermore, molecular docking and subsequent molecular dynamics simulations provided structural validation, revealing favorable binding energies and stable interactions for representative

compound-target pairs, such as Naringenin with SIRT1 and MMP14, and Compound 85699751 with Erbb2, suggesting plausible molecular mechanisms for the observed activities. Therefore, the integration of computational predictions with robust in vivo and in vitro experimental validation confirms ARR's significant anti-inflammatory and analgesic properties relevant to OA, providing a strong basis for further mechanistic studies.

CRediT authorship contribution statement

Hee-Geun Jo: Writing – review & editing, Writing – original draft, Visualization, Validation, Software, Resources, Project administration, Methodology, Investigation, Formal analysis, Data curation, Conceptualization. **Chae Yun Baek:** Writing – review & editing, Writing – original draft, Validation, Software, Resources, Methodology, Investigation, Formal analysis, Data curation, Conceptualization. **Sidra Ilyas:** Visualization, Software, Methodology, Investigation, Data curation. **Yeseul Hwang:** Investigation, Data curation. **Eunhye Baek:** Writing – review & editing, Writing – original draft. **Ho Sueb Song:** Writing – review & editing, Supervision, Funding acquisition. **Donghun Lee:** Writing – review & editing, Supervision, Project administration, Funding acquisition.

Informed consent statement

Not applicable.

Institutional review board statement

The Gachon University Center of Animal Care and Use approved all of the experiments listed above (GU1-2022-IA0071-01), approval on 2023.08.07.

Data availability statement

All data from this study are included in the main body of the article and in the supplementary files. Uncropped Western blot data are provided in Supplementary Material S12.

Declaration of generative AI and AI-assisted technologies in the writing process

The preparation of this work was not assisted by any form of generative artificial intelligence. It is hereby declared that all sentences, figures, and tables in the manuscript were written, reviewed, and edited by the human authors.

Funding

This research was supported by the Basic Science Research Program through the National Research Foundation of Korea (NRF), funded by the Ministry of Education (RS-2023-00247663); This work was supported by the National Research Foundation of Korea (NRF) grant funded by the Korea government (MSIT) (RS-2025-00523080).

Declaration of competing interest

The authors declare this research was conducted absent any commercial/financial relationships interpretable as a potential conflict of interest.

In addition, there is no significant financial support that could influence the outcome of this study.

Acknowledgments

We would like to thank Editage (www.editage.co.kr) for English language editing.

Appendix A. Supplementary data

Supplementary data to this article can be found online at https://doi.org/10.1016/j.jep.2025.119915.

Data availability

All data from this study are included in the main body of the article and in the supplementary files

References

Abraham, M.J., Murtola, T., Schulz, R., Páll, S., Smith, J.C., Hess, B., Lindahl, E., 2015. GROMACS: high performance molecular simulations through multi-level parallelism from laptops to supercomputers. SoftwareX 1–2, 19–25. https://doi.org/10.1016/j.softx.2015.06.001.

Amberger, J.S., Bocchini, C.A., Scott, A.F., Hamosh, A., 2019. OMIM.org: leveraging knowledge across phenotype-gene relationships. Nucleic Acids Res. 47, D1038–D1043. https://doi.org/10.1093/nar/gky1151.

Ansari, M.M., Ghosh, M., Lee, D.-S., Son, Y.-O., 2024. Senolytic therapeutics: an emerging treatment modality for osteoarthritis. Ageing Res. Rev. 96, 102275. https://doi.org/10.1016/j.arr.2024.102275.

Bjurström, M.F., Blennow, K., Zetterberg, H., Bodelsson, M., Waldén, M., Dietz, N., Hall, S., Hansson, O., Irwin, M.R., Mattsson-Carlgren, N., 2022. Central nervous system monoaminergic activity in hip osteoarthritis patients with disabling pain: associations with pain severity and central sensitization. Pain Rep 7, e988. https://doi.org/10.1097/PR9.0000000000000988.

Bussi, G., Donadio, D., Parrinello, M., 2007. Canonical sampling through velocity rescaling. J. Chem. Phys. 126, 014101. https://doi.org/10.1063/1.2408420.

Cai, J., Wen, H., Zhou, H., Zhang, D., Lan, D., Liu, S., Li, C., Dai, X., Song, T., Wang, X., He, Y., He, Z., Tan, J., Zhang, J., 2023. Naringenin: a flavanone with anti-inflammatory and anti-infective properties. Biomed. Pharmacother. Biomedecine Pharmacother. 164, 114990. https://doi.org/10.1016/j.biopha.2023.114990.

Chaib, S., Tchkonia, T., Kirkland, J.L., 2022. Cellular senescence and senolytics: the path to the clinic. Nat. Med. 28, 1556–1568. https://doi.org/10.1038/s41591-022-01923-y.

Chin, C.-H., Chen, S.-H., Wu, H.-H., Ho, C.-W., Ko, M.-T., Lin, C.-Y., 2014. cytoHubba: identifying hub objects and sub-networks from complex interactome. BMC Syst. Biol. 8, S11. https://doi.org/10.1186/1752-0509-8-S4-S11.

Daina, A., Michielin, O., Zoete, V., 2019. SwissTargetPrediction: updated data and new features for efficient prediction of protein targets of small molecules. Nucleic Acids Res. 47, W357–W364. https://doi.org/10.1093/nar/gkz382.

Daina, A., Michielin, O., Zoete, V., 2017. SwissADME: a free web tool to evaluate pharmacokinetics, drug-likeness and medicinal chemistry friendliness of small molecules. Sci. Rep. 7, 42717. https://doi.org/10.1038/srep42717.

De Roover, A., Escribano-Núñez, A., Monteagudo, S., Lories, R., 2023. Fundamentals of osteoarthritis: inflammatory mediators in osteoarthritis. Osteoarthr. Cartil. 31, 1303–1311. https://doi.org/10.1016/j.joca.2023.06.005.

Dvir-Ginzberg, M., Steinmeyer, J., 2013. Towards elucidating the role of SirT1 in osteoarthritis. Front. Biosci. (Landmark Ed.) 18, 343–355. https://doi.org/10.2741/4105.

Essmann, U., Perera, L., Berkowitz, M.L., Darden, T., Lee, H., Pedersen, L.G., 1995. A smooth particle mesh Ewald method. J. Chem. Phys. 103, 8577–8593. https://doi.org/10.1063/1.470117.

Fang, S., Zhang, B., Xiang, W., Zheng, L., Wang, X., Li, S., Zhang, T., Feng, D., Gong, Y., Wu, J., Yuan, J., Wu, Y., Zhu, Y., Liu, E., Ni, Z., 2024. Natural products in osteoarthritis treatment: bridging basic research to clinical applications. Chin. Med. 19, 25. https://doi.org/10.1186/s13020-024-00899-w.

Gordon, G.M., Ledee, D.R., Feuer, W., Fini, M.E., 2009. Cytokines and signaling pathways regulating matrix Metalloproteinase-9 (MMP-9) expression in corneal epithelial cells. J. Cell. Physiol. 221, 402–411. https://doi.org/10.1002/jcp.21869.

Grillet, B., Pereira, R.V.S., Van Damme, J., Abu El-Asrar, A., Proost, P., Opdenakker, G., 2023. Matrix metalloproteinases in arthritis: towards precision medicine. Nat. Rev. Rheumatol. 19, 363–377. https://doi.org/10.1038/s41584-023-00966-w.

Haseeb, A., Chen, D., Haqqi, T.M., 2013. Delphinidin inhibits IL-1β-induced activation of NF-κB by modulating the phosphorylation of IRAK-1Ser376 in human articular chondrocytes. Rheumatol. Oxf. Engl. 52, 998–1008. https://doi.org/10.1093/rheumatology/kes363.

Hou, D., Lin, H., Feng, Y., Zhou, K., Li, X., Yang, Y., Wang, S., Yang, X., Wang, J., Zhao, H., Zhang, X., Fan, J., Lu, S., Wang, D., Zhu, L., Ju, D., Chen, Y.Z., Zeng, X., 2023. CMAUP database update 2024: extended functional and association information of useful plants for biomedical research. Nucleic Acids Res. gkad921. https://doi.org/10.1093/nar/gkad921.

Housmans, B.a.C., Neefjes, M., Surtel, D.a.M., Vitík, M., Cremers, A., van Rhijn, L.W., van der Kraan, P.M., van den Akker, G.G.H., Welting, T.J.M., 2022. Synovial fluid from end-stage osteoarthritis induces proliferation and fibrosis of articular chondrocytes via MAPK and RhoGTPase signaling. Osteoarthr. Cartil. 30, 862–874. https://doi.org/10.1016/j.joca.2021.12.015.

Huang, J., MacKerell, A.D., 2013. CHARMM36 all-atom additive protein force field: validation based on comparison to NMR data. J. Comput. Chem. 34, 2135–2145. https://doi.org/10.1002/jcc.23354.
Jamal, N., Hollabaugh, W., Scott, L., Takkouche, S., 2025. Unravelling the ties that bind: the intersection of obesity, osteoarthritis, and inflammatory pathways with emphasis on glucagon-like peptide-1 agonists. Clin. Obes. 15, e12700. https://doi.org/10.1111/cob.12700.
Jang, M.-K., Kim, H.S., Chung, Y.-H., 2014. Clinical aspects of tumor necrosis factor-α signaling in hepatocellular carcinoma. Curr. Pharm. Des. 20, 2799–2808. https://doi.org/10.2174/13816128113199990587.
Jiang, Y.-P., Wen, J.-J., Zhao, X.-X., Gao, Y.-C., Ma, X., Song, S.-Y., Jin, Y., Shao, T.-J., Yu, J., Wen, C.-P., 2022. The flavonoid naringenin alleviates collagen-induced arthritis through curbing the migration and polarization of CD4+ T lymphocyte driven by regulating mitochondrial fission. Int. J. Mol. Sci. 24, 279. https://doi.org/10.3390/ijms24010279.
Jing, Y., Zhang, Y.-F., Shang, M.-Y., Liu, G.-X., Li, Y.-L., Wang, X., Cai, S.-Q., 2017. Chemical constituents from the roots and rhizomes of Asarum heterotropoides Var. mandshuricum and the in vitro anti-inflammatory activity. Mol. Basel Switz. 22, 125. https://doi.org/10.3390/molecules22010125.
Jo, H.G., Baek, C.Y., Kim, D., Kim, S., Han, Y., Park, C., Song, H.S., Lee, D., 2023. Network analysis, in vivo, and in vitro experiments identified the mechanisms by which Piper longum L. [piperaceae] alleviates cartilage destruction, joint inflammation, and arthritic pain. Front. Pharmacol. 14, 1282943. https://doi.org/10.3389/fphar.2023.1282943.
Jo, H.-G., Baek, C.Y., Kim, D., Lee, D., Song, H.S., 2023. Stem of Sorbus commixta hedl. Extract inhibits cartilage degradation and arthritic pain in experimental model via anti-inflammatory activity. Nutrients 15, 3774. https://doi.org/10.3390/nu15173774.
Jo, H.-G., Baek, C.Y., Lee, J., Hwang, Y., Baek, E., Hwang, J.H., Lee, D., 2024a. Anti-inflammatory, analgesic, functional improvement, and chondroprotective effects of erigeron breviscapus (vant.) hand.-mazz. Extract in osteoarthritis: an in vivo and in vitro study. Nutrients 16, 1035. https://doi.org/10.3390/nu16071035.
Jo, H.-G., Baek, C.-Y., Song, H.S., Lee, D., 2024b. Network pharmacology and experimental verifications to discover Scutellaria baicalensis georgi's effects on joint inflammation, destruction, and pain in osteoarthritis. Int. J. Mol. Sci. 25, 2127. https://doi.org/10.3390/ijms25042127.
Jo, H.-G., Lee, G.-Y., Baek, C.Y., Song, H.S., Lee, D., 2020. Analgesic and anti-inflammatory effects of Aucklandia lappa root extracts on acetic acid-induced writhing in mice and monosodium iodoacetate-induced osteoarthritis in rats. Plants Basel Switz 10, 42. https://doi.org/10.3390/plants10010042.
Jo, H.-G., Seo, J., Baek, E., Lee, D., 2025. Exploring the benefits and prescribing informations of combining East Asian herbal medicine with conventional medicine in the treatment of rheumatoid arthritis: a systematic review and multifaceted analysis of 415 randomized controlled trials. Pharmacol. Res. 212, 107616. https://doi.org/10.1016/j.phrs.2025.107616.
Jo, H.-G., Seo, J., Lee, D., 2022. Clinical evidence construction of East Asian herbal medicine for inflammatory pain in rheumatoid arthritis based on integrative data mining approach. Pharmacol. Res. 185, 106460. https://doi.org/10.1016/j.phrs.2022.106460.
Kanehisa, M., Sato, Y., Kawashima, M., 2022. KEGG mapping tools for uncovering hidden features in biological data. Protein Sci. Publ. Protein Soc. 31, 47–53. https://doi.org/10.1002/pro.4172.
Kaneko, K., Williams, R.O., Dransfield, D.T., Nixon, A.E., Sandison, A., Itoh, Y., 2016. Selective inhibition of membrane type 1 matrix metalloproteinase abrogates progression of experimental inflammatory arthritis: synergy with tumor necrosis factor blockade. Arthritis Rheumatol. Hoboken NJ 68, 521–531. https://doi.org/10.1002/art.39414.
Katz, J.N., Arant, K.R., Loeser, R.F., 2021. Diagnosis and treatment of hip and knee osteoarthritis: a review. JAMA 325, 568–578. https://doi.org/10.1001/jama.2020.22171.
Kauppinen, A., Suuronen, T., Ojala, J., Kaarniranta, K., Salminen, A., 2013. Antagonistic crosstalk between NF-κB and SIRT1 in the regulation of inflammation and metabolic disorders. Cell. Signal. 25, 1939–1948. https://doi.org/10.1016/j.cellsig.2013.06.007.
Latourte, A., Kloppenburg, M., Richette, P., 2020. Emerging pharmaceutical therapies for osteoarthritis. Nat. Rev. Rheumatol. 16, 673–688. https://doi.org/10.1038/s41584-020-00518-6.
Li, Wenhao, Yu, L., Li, Wenming, Ge, G., Ma, Y., Xiao, L., Qiao, Y., Huang, Wei, Huang, Wenli, Wei, M., Wang, Z., Bai, J., Geng, D., 2023. Prevention and treatment of inflammatory arthritis with traditional Chinese medicine: underlying mechanisms based on cell and molecular targets. Ageing Res. Rev. 89, 101981. https://doi.org/10.1016/j.arr.2023.101981.
Li, X., Ren, J., Zhang, W., Zhang, Z., Yu, J., Wu, J., Sun, H., Zhou, S., Yan, K., Yan, X., Wang, W., 2022. LTM-TCM: a comprehensive database for the linking of traditional Chinese medicine with modern medicine at molecular and phenotypic levels. Pharmacol. Res. 178, 106185. https://doi.org/10.1016/j.phrs.2022.106185.
Liu, H., Wang, C., 2022. The genus asarum: a review on phytochemistry, ethnopharmacology, toxicology and pharmacokinetics. J. Ethnopharmacol. 282, 114642. https://doi.org/10.1016/j.jep.2021.114642.
Long, H., Liu, Q., Yin, H., Wang, K., Diao, N., Zhang, Y., Lin, J., Guo, A., 2022. Prevalence trends of site-specific osteoarthritis from 1990 to 2019: findings from the global burden of disease study 2019. Arthritis Rheumatol. Hoboken NJ 74, 1172–1183. https://doi.org/10.1002/art.42089.
Lu, H., Su, H., Liu, Y., Yin, K., Wang, D., Li, B., Wang, Y., Xing, M., 2022. NLRP3 inflammasome is involved in the mechanism of the mitigative effect of lycopene on sulfamethoxazole-induced inflammatory damage in grass carp kidneys. Fish Shellfish Immunol. 123, 348–357. https://doi.org/10.1016/j.fsi.2022.03.018.
Lu, H., Zhao, H., Wang, Y., Guo, M., Mu, M., Liu, Y., Nie, X., Huang, P., Xing, M., 2021. Arsenic (III) induces oxidative stress and inflammation in the gills of common carp, which is ameliorated by zinc (II). J. Inorg. Biochem. 225, 111617. https://doi.org/10.1016/j.jinorgbio.2021.111617.
Mahmoudian, A., Lohmander, L.S., Mobasheri, A., Englund, M., Luyten, F.P., 2021. Early-stage symptomatic osteoarthritis of the knee - time for action. Nat. Rev. Rheumatol. 17, 621–632. https://doi.org/10.1038/s41584-021-00673-4.
Moulin, D., Sellam, J., Berenbaum, F., Guicheux, J., Boutet, M.-A., 2025. The role of the immune system in osteoarthritis: mechanisms, challenges and future directions. Nat. Rev. Rheumatol. 21, 221–236. https://doi.org/10.1038/s41584-025-01223-y.
Paiola, M., Portnoy, D.M., Hao, L.Y., Bukhari, S., Winchester, R.J., Henick, B.S., Mor, A., Gartshteyn, Y., 2025. Osteoarthritis increases the risk of inflammatory arthritis due to immune checkpoint inhibitors associated with tissue-resident memory T cells. J. Immunother. Cancer 13, e010758. https://doi.org/10.1136/jitc-2024-010758.
Pan, Z., He, Q., Zeng, J., Li, S., Li, M., Chen, B., Yang, J., Xiao, J., Zeng, C., Luo, H., Wang, H., 2022. Naringenin protects against iron overload-induced osteoarthritis by suppressing oxidative stress. Phytomedicine Int. J. Phytother. Phytopharm. 105, 154330. https://doi.org/10.1016/j.phymed.2022.154330.
Panossian, A., Lemerond, T., Efferth, T., 2024. State-of-the-Art review on botanical hybrid preparations in phytomedicine and phytotherapy research: background and perspectives. Pharm. Basel Switz. 17, 483. https://doi.org/10.3390/ph17040483.
Panossian, A., Seo, E.-J., Wikman, G., Efferth, T., 2015. Synergy assessment of fixed combinations of herba andrographidis and Radix eleutherococci extracts by transcriptome-wide microarray profiling. Phytomedicine Int. J. Phytother. Phytopharm. 22, 981–992. https://doi.org/10.1016/j.phymed.2015.08.004.
Panossian, A.G., Efferth, T., Shikov, A.N., Pozharitskaya, O.N., Kuchta, K., Mukherjee, P. K., Banerjee, S., Heinrich, M., Wu, W., Guo, D.-A., Wagner, H., 2021. Evolution of the adaptogenic concept from traditional use to medical systems: pharmacology of stress- and aging-related diseases. Med. Res. Rev. 41, 630–703. https://doi.org/10.1002/med.21743.
Piñero, J., Bravo, À., Queralt-Rosinach, N., Gutiérrez-Sacristán, A., Deu-Pons, J., Centeno, E., García-García, J., Sanz, F., Furlong, L.I., 2017. DisGeNET: a comprehensive platform integrating information on human disease-associated genes and variants. Nucleic Acids Res. 45, D833–D839. https://doi.org/10.1093/nar/gkw943.
Piñero, J., Ramírez-Anguita, J.M., Saüch-Pitarch, J., Ronzano, F., Centeno, E., Sanz, F., Furlong, L.I., 2020. The DisGeNET knowledge platform for disease genomics: 2019 update. Nucleic Acids Res. 48, D845–D855. https://doi.org/10.1093/nar/gkz1021.
Robinson, W.H., Lepus, C.M., Wang, Q., Raghu, H., Mao, R., Lindstrom, T.M., Sokolove, J., 2016. Low-grade inflammation as a key mediator of the pathogenesis of osteoarthritis. Nat. Rev. Rheumatol. 12, 580–592. https://doi.org/10.1038/nrrheum.2016.136.
Ru, J., Li, Peng, Wang, J., Zhou, W., Li, B., Huang, C., Li, Pidong, Guo, Z., Tao, W., Yang, Y., Xu, X., Li, Y., Wang, Y., Yang, L., 2014. TCMSP: a database of systems pharmacology for drug discovery from herbal medicines. J. Cheminformatics 6, 13. https://doi.org/10.1186/1758-2946-6-13.
Sabio, G., Davis, R.J., 2014. TNF and MAP kinase signaling pathways. Semin. Immunol. 26, 237–245. https://doi.org/10.1016/j.smim.2014.02.009.
Sanchez-Lopez, E., Coras, R., Torres, A., Lane, N.E., Guma, M., 2022. Synovial inflammation in osteoarthritis progression. Nat. Rev. Rheumatol. 18, 258–275. https://doi.org/10.1038/s41584-022-00749-9.
Scott, A.J., Ellison, M., Sinclair, D.A., 2021. The economic value of targeting aging. Nat. Aging 1, 616–623. https://doi.org/10.1038/s43587-021-00080-0.
Shannon, P., Markiel, A., Ozier, O., Baliga, N.S., Wang, J.T., Ramage, D., Amin, N., Schwikowski, B., Ideker, T., 2003. Cytoscape: a software environment for integrated models of biomolecular interaction networks. Genome Res. 13, 2498–2504. https://doi.org/10.1101/gr.1239303.
Stelzer, G., Rosen, N., Plaschkes, I., Zimmerman, S., Twik, M., Fishilevich, S., Stein, T.I., Nudel, R., Lieder, I., Mazor, Y., Kaplan, S., Dahary, D., Warshawsky, D., Guan-Golan, Y., Kohn, A., Rappaport, N., Safran, M., Lancet, D., 2016. The GeneCards suite: from gene data mining to disease genome sequence analyses. Curr. Protoc. Bioinforma. 54 (1.30.1–1.30.33). https://doi.org/10.1002/cpbi.5.
Su, J., Yu, M., Wang, H., Wei, Y., 2023. Natural anti-inflammatory products for osteoarthritis: from molecular mechanism to drug delivery systems and clinical trials. Phytother. Res. PTR 37, 4321–4352. https://doi.org/10.1002/ptr.7935.
Tchkonia, T., Palmer, A.K., Kirkland, J.L., 2021. New Horizons: Novel approaches to enhance healthspan through targeting cellular senescence and related aging mechanisms. J. Clin. Endocrinol. Metab. 106, e1481–e1487. https://doi.org/10.1210/clinem/dgaa728.
The UniProt Consortium, 2021. UniProt: the universal protein knowledgebase in 2021. Nucleic Acids Res. 49, D480–D489. https://doi.org/10.1093/nar/gkaa1100.
van Helvoort, E.M., Welsing, P.M.J., Jansen, M.P., Gielis, W.P., Loef, M., Kloppenburg, M., Blanco, F., Haugen, I.K., Berenbaum, F., Bay-Jensen, A.-C., Ladel, C., Lalande, A., Larkin, J., Loughlin, J., Mobasheri, A., Weinans, H., Lafeber, F., Eijkelkamp, N., Mastbergen, S., 2021. Neuropathic pain in the IMI-APPROACH knee osteoarthritis cohort: prevalence and phenotyping. RMD Open 7, e002025. https://doi.org/10.1136/rmdopen-2021-002025.
Van Spil, W.E., Kubassova, O., Boesen, M., Bay-Jensen, A.-C., Mobasheri, A., 2019. Osteoarthritis phenotypes and novel therapeutic targets. Biochem. Pharmacol. 165, 41–48. https://doi.org/10.1016/j.bcp.2019.02.037.
Wang, J., Niu, X., Wu, C., Wu, D., 2018. Naringenin modifies the development of lineage-specific effector CD4+ T cells. Front. Immunol. 9, 2267. https://doi.org/10.3389/fimmu.2018.02267.

Wang, P., Guan, P.-P., Guo, C., Zhu, F., Konstantopoulos, K., Wang, Z.-Y., 2013. Fluid shear stress-induced osteoarthritis: roles of cyclooxygenase-2 and its metabolic products in inducing the expression of proinflammatory cytokines and matrix metalloproteinases. FASEB J. Off. Publ. Fed. Am. Soc. Exp. Biol. 27, 4664–4677. https://doi.org/10.1096/fj.13-234542.

Wang, P., Qian, H., Xiao, M., Lv, J., 2023. Role of signal transduction pathways in IL-1β-induced apoptosis: pathological and therapeutic aspects. Immun. Inflamm. Dis. 11, e762. https://doi.org/10.1002/iid3.762.

Wang, R., Hou, L., Lu, H., Zhang, Y., Guo, T., Zhou, B., Zhao, H., Xing, M., 2024. Unveiling the interplay of MAPK/NF-κB/MLKL axis in brain health: omega-3 as a promising candidates against copper neurotoxicity. J. Environ. Manage. 370, 122791. https://doi.org/10.1016/j.jenvman.2024.122791.

Wen, Z., Qiu, L., Ye, Z., Tan, X., Xu, X., Lu, M., Kuang, G., 2024. The role of Th/Treg immune cells in osteoarthritis. Front. Immunol. 15. https://doi.org/10.3389/fimmu.2024.1393418.

Weng, Q., Chen, Q., Jiang, T., Zhang, Y., Zhang, W., Doherty, M., Xie, J., Liu, K., Li, J., Yang, T., Wei, J., Lei, G., Zeng, C., 2024. Global burden of early-onset osteoarthritis, 1990-2019: results from the global burden of disease study 2019. Ann. Rheum. Dis. https://doi.org/10.1136/ard-2023-225324 ard-2023-225324.

Wishart, D.S., Feunang, Y.D., Guo, A.C., Lo, E.J., Marcu, A., Grant, J.R., Sajed, T., Johnson, D., Li, C., Sayeeda, Z., Assempour, N., Iynkkaran, I., Liu, Y., Maciejewski, A., Gale, N., Wilson, A., Chin, L., Cummings, R., Le, D., Pon, A., Knox, C., Wilson, M., 2018. DrugBank 5.0: a major update to the DrugBank database for 2018. Nucleic Acids Res. 46, D1074–D1082. https://doi.org/10.1093/nar/gkx1037.

Wu, S., Guo, W., Chen, L., Lin, X., Tang, M., Lin, C., Guo, H., Zhang, T., Gao, Y., 2024. Downregulation of Gadd45β alleviates osteoarthritis by repressing lipopolysaccharide-induced fibroblast-like synoviocyte inflammation, proliferation and migration. Int. Immunopharmacol. 126, 111202. https://doi.org/10.1016/j.intimp.2023.111202.

Yamamoto, K., Santamaria, S., Botkjaer, K.A., Dudhia, J., Troeberg, L., Itoh, Y., Murphy, G., Nagase, H., 2017. Inhibition of shedding of low-density lipoprotein receptor-related protein 1 reverses cartilage matrix degradation in osteoarthritis. Arthritis Rheumatol. Hoboken NJ 69, 1246–1256. https://doi.org/10.1002/art.40080.

Yang, D., Chen, Y., Guo, J., Xu, X., Yang, M., Xie, J., Xu, K., Xu, P., 2024. The organ-joint axes in osteoarthritis: significant pathogenesis and therapeutic targets. Aging Dis. https://doi.org/10.14336/AD.2024.1223.

Yao, Q., Wu, X., Tao, C., Gong, W., Chen, M., Qu, M., Zhong, Y., He, T., Chen, S., Xiao, G., 2023. Osteoarthritis: pathogenic signaling pathways and therapeutic targets. Signal Transduct. Target. Ther. 8, 56. https://doi.org/10.1038/s41392-023-01330-w.

Zeng, X., Zhang, P., Wang, Y., Qin, C., Chen, S., He, W., Tao, L., Tan, Y., Gao, D., Wang, B., Chen, Z., Chen, W., Jiang, Y.Y., Chen, Y.Z., 2019. CMAUP: a database of collective molecular activities of useful plants. Nucleic Acids Res. 47, D1118–D1127. https://doi.org/10.1093/nar/gky965.

Zhang, W., Zhang, J., Zhang, M., Nie, L., 2014. Protective effect of asarum extract in rats with adjuvant arthritis. Exp. Ther. Med. 8, 1638–1642. https://doi.org/10.3892/etm.2014.1941.

Zhang, Y., Li, X., Shi, Y., Chen, T., Xu, Z., Wang, P., Yu, M., Chen, W., Li, B., Jing, Z., Jiang, H., Fu, L., Gao, W., Jiang, Y., Du, X., Gong, Z., Zhu, W., Yang, H., Xu, H., 2023. ETCM v2.0: an update with comprehensive resource and rich annotations for traditional Chinese medicine. Acta Pharm. Sin. B 13, 2559–2571. https://doi.org/10.1016/j.apsb.2023.03.012.

Zhou, Y., Zhou, B., Pache, L., Chang, M., Khodabakhshi, A.H., Tanaseichuk, O., Benner, C., Chanda, S.K., 2019. Metascape provides a biologist-oriented resource for the analysis of systems-level datasets. Nat. Commun. 10, 1523. https://doi.org/10.1038/s41467-019-09234-6.

Zhou, Ying, Zhang, Y., Zhao, D., Yu, X., Shen, X., Zhou, Yuan, Wang, S., Qiu, Y., Chen, Y., Zhu, F., 2023. TTD: therapeutic target database describing target druggability information. Nucleic Acids Res. gkad751. https://doi.org/10.1093/nar/gkad751.

Zhu, L., Bi, Y., Liang, T., Zhang, P., Xiao, X., Yu, T., 2025. Ginkgetin delays the progression of osteoarthritis by inhibiting the NF-κB and MAPK signaling pathways. J. Orthop. Surg. 20, 139. https://doi.org/10.1186/s13018-025-05525-5.